Open Access Articles

Simulating extreme total water levels using a time-dependent, extreme value approach

RESEARCH ARTICLE

Simulating extreme total water levels using a time-dependent, extreme value approach

Katherine A. Serafin[1] and Peter Ruggiero[1]

[1]College of Earth, Ocean, and Atmospheric Sciences, Oregon State University, Corvallis, Oregon, USA

Abstract Coastal flood hazard zones and the design of coastal defenses are often devised using the maximum recorded water level or a "design" event such as the 100 year return level, usually projected from observed extremes. Despite technological advances driving more consistent instrumental records of waves and water levels, the observational record may be short, punctuated with intermittent gaps, and vary in quality. These issues in the record often preclude accurate and robust estimates of extreme return level events. Here we present a total water level full simulation model (TWL-FSM) that simulates the various components of TWLs (waves, tides, and nontidal residuals) in a Monte Carlo sense, taking into account conditional dependencies that exist between the various components. Extreme events are modeled using nonstationary extreme value distributions that include seasonality and climate variability. The resulting synthetic TWLs allow for empirical extraction of return level events and the ability to more robustly estimate and assess present-day flood and erosion hazards. The approach is demonstrated along a northern Oregon, USA littoral cell but is applicable to beaches anywhere wave and water level records or hindcasts are available. Simulations result in extreme 100 year TWL return levels as much as 90 cm higher than those extrapolated from the "observational" record. At the Oregon site, this would result in 30% more coastal flooding than the "observational" 100 year TWL return level projections. More robust estimates of extreme TWLs and tighter confidence bounds on return level events can aid coastal engineers, managers, and emergency planners in evaluating exposure to hazards.

1. Introduction

The coastline is one of the most dynamic environments on earth, where the combination of winds, waves, currents, and high water levels alter coastal morphology over a wide range of time scales. Forcing that results in morphological evolution ranges from millennial variability in sea level to winter storms producing high waves and surges that can dramatically change the coastline in a matter of hours. In the U.S. alone, 30% of the population lives bordering open ocean or associated water bodies [*Crowell et al.*, 2007] and as much as 3% of the population living in these coastal zones are at risk from the 100 year coastal flooding event [*Crowell et al.*, 2010]. The high percentage of people living and recreating along the coastline creates an increasingly vulnerable population to coastal hazards. Accurate representations of not only the high level of natural variability of the coastal system but also the potential impacts of human-induced climate change are needed to improve our knowledge of coastal risk.

Significant effort has been directed toward detecting and understanding the temporally and spatially variable accelerating trends in global mean sea level rise (SLR) [e.g., *Church and White*, 2006, 2011; *Cazenave et al.*, 2014] influenced by processes in the ocean, atmosphere, and cryosphere [e.g., *Menéndez and Woodworth*, 2010; *Sallenger et al.*, 2012]. Changing patterns of interannual climate variability (e.g., El Niño Southern Oscillation (ENSO)) [*Santoso et al.*, 2013] and storm frequency and intensity [*Graham and Diaz*, 2001; *Knutson et al.*, 2010; *Wang et al.*, 2014], possibly attributed to global climate change [*Graham and Diaz*, 2001; *Emanuel*, 2013; *Cai et al.*, 2014], has the ability to increase the range of coastline at risk to flooding and erosion events when combined with accelerating SLR trends. Therefore, while understanding and predicting the range and variability in SLR is important, it is the coincidence of high water levels and storm-induced waves that often results in extreme inundation and erosion along vulnerable coastlines [*Ruggiero et al.*, 1996, 2001; *Sallenger*, 2000; *Woodruff et al.*, 2013].

Extreme value analysis has been developed to quantify a behavior or process at unusually large or small levels and to project the probability of the occurrence of these events [*Gumbel*, 1958; *Leadbetter et al.*, 1983;

Coles, 2001]. Multiple methods have been proposed for different environmental variables including the annual maxima method [*Gumbel*, 1958; *Coles*, 2001; *Smith*, 2001], the r-largest maxima [*Smith*, 1986], and the peak-over threshold approach [*Smith*, 1989; *Davison and Smith*, 1990]. These extreme value approaches for estimating return levels from instrumental records depend largely on the record length, which must be sufficiently long. Statistically, longer records imply smaller standard errors, and meteorologically, the record should be long enough to encompass the full range of variability in extremes. For processes that result from the combination of two or more individual processes, extremes can only be computed based on the length of the shortest individual record. For example, extreme total water level (TWL) return levels, produced by the combination of the mean sea level, the deterministic astronomical tide, nontidal residuals, and storm wave-induced water level variations [e.g., *Sallenger*, 2000; *Ruggiero et al.*, 2001], may be biased low if the maximum recorded nontidal residuals occurred before the wave measurement record begins or if both records are relatively short.

Circumventing the problem of records limited by gaps, full simulation, probabilistic methods have begun to be incorporated with extreme event modeling to produce thousands of estimates of wave climates and/or water levels for robust statistics on extremes [*Hawkes et al.*, 2002; *Garrity et al.*, 2006; *Callaghan et al.*, 2008; *Goring et al.*, 2010; *Li et al.*, 2014; *Gouldby et al.*, 2014]. In tide or surge dominated environments, emphasis is placed on simulating only water levels [*Goring et al.*, 2010; *Zhang and Sheng*, 2013], while in other locations, where large wave events enhance the elevation of flooding events, the wave climate is also simulated [*Callaghan et al.*, 2008; *Li et al.*, 2014; *Gouldby et al.*, 2014]. Due to the interrelatedness of many of these simulated variables (e.g., large wave heights and storm surges are often generated by the same meteorological systems) special care is taken to model the dependencies between variables [*Hawkes et al.*, 2002; *Callaghan et al.*, 2008; *Corbella and Stretch*, 2013; *Li et al.*, 2014; *Gouldby et al.*, 2014]. While each of these simulation methods utilizes extreme value theory to model the extreme events, they consider the population of extremes to be stationary, and have thus far ignored nonstationary drivers of extremes such as the effects of seasonality or ENSO.

Our focus here is on extreme TWLs on sandy beaches. In order to analyze extreme events produced by a combination of factors, the TWL is first calculated by combining each of the "observational" TWL components (tide, nontidal residuals, and storm wave-induced water level variations). TWL return levels can then be extracted from extreme value distribution fits to the combination of components instead of to the extremes of the individual components. However, because extreme TWLs are a combination of a wide range of variables, there is a likelihood that coastlines have not experienced the co-occurrence of the maximum level of astronomical tide, nontidal residuals, and wave-induced water levels over the relatively short instrumental record length. To address these limitations, we develop a time-dependent, full simulation TWL model (TWL-FSM) that can be applied to coastal defense design and flood hazard risk assessments. We first fit independent, extreme significant wave heights (SWHs) and nontidal residuals to nonstationary extreme value distributions. Next, we simulate multiple, synthetic records of arbitrary length, for each of the TWL components. Each component of the TWL is simulated based on approximately 30 or more years of data, and includes the joint dependencies between respective TWL components. These simulations produce various combinations of events and more robust estimates of TWL return levels. We then can compare TWL return levels extracted from the synthetic records to those extrapolated from the "observational" record's extreme value distribution fit. While this manuscript is primarily intended to highlight the methodology of the full simulation model, an example of the applicability of the model is demonstrated along a representative littoral cell for northern Oregon, USA.

1.1. Application Area

The methodologies presented in this paper can be applied to a range of coastlines that have wave and water level measurements or hindcasts available; here we choose to apply it to a sandy coastline in Oregon, USA (Figure 1). The Oregon coastline is essentially a series of discrete littoral cells segmented by large, erosion resistant headlands [*Komar*, 1998]. The Rockaway littoral cell, a representative littoral cell in northern Oregon, is a 30 km stretch of coastline between Cape Falcon and Cape Meares, two headlands that extend offshore into deep water (Figure 1c). Century and decadal-scale shoreline change rates for this cell are quite variable [*Ruggiero et al.*, 2013]; however, coastal retreat rates approach 2.0 m/yr along the most developed section of coast. Hot spot erosion to the Rockaway cell due to storms during the major El Niño of 1997–1998 and the severe winter of 1998–1999 have left the coastline in a degraded state [*Allan and Komar*, 2002]. Since
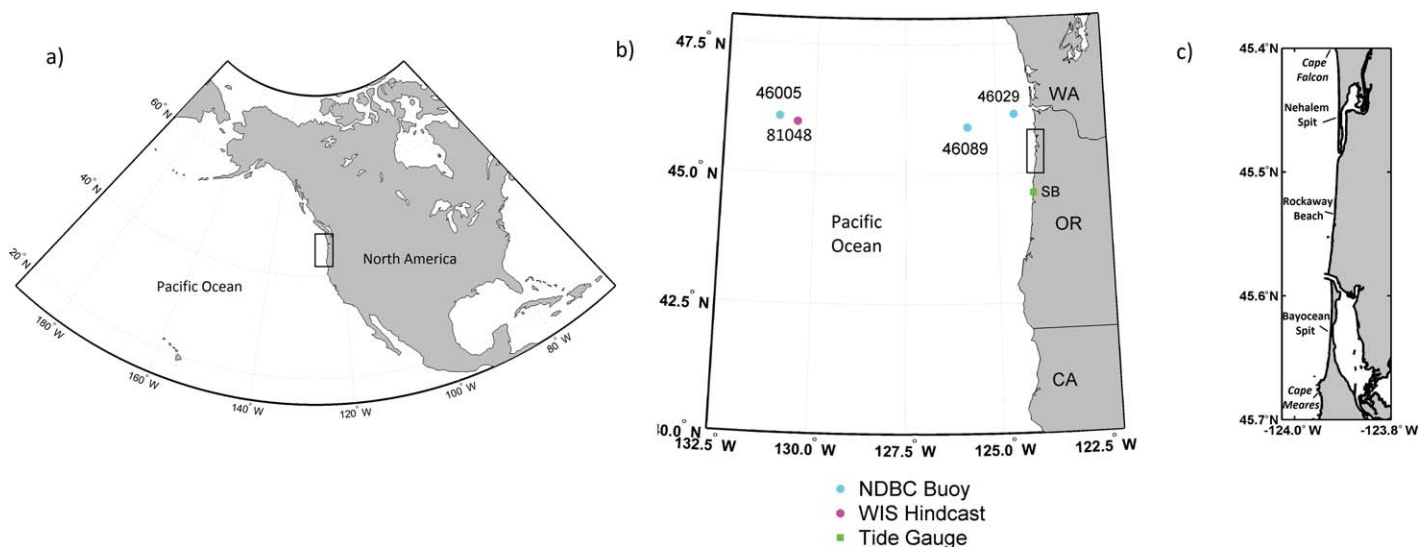
Figure 1. (a) Location of region of study (inset) in North America, (b) Region of study, the Pacific Northwest (PNW) with (c) Rockaway, Oregon littoral cell inset. Locations of NDBC buoys (cyan), the WIS hindcast (magenta), and NOAA tide gauge (green) used to compute the hourly "observational" TWL record are also displayed.

persistent erosion has begun to threaten local infrastructure, we apply our TWL simulation model to this coastline to evaluate both chronic and extreme coastal flood and coastal change hazards in this location.

2. Methods

Below we present methods for (1) developing a continuous, hourly "observational" time series for each TWL component, (2) evaluating extreme TWLs in the context of *Sallenger*'s [2000] storm impact scale to assess exposure of the Rockaway, Oregon littoral cell to coastal erosion and flooding, (3) modeling both stationary and nonstationary extreme events, and (4) simulating each TWL component for more robust estimates of the range of extreme events.

2.1. Development of an "Observational" TWL Time Series

At any given time, the elevation of the TWL is comprised of four components such that

$$TWL = MSL + \eta_A + \eta_{NTR} + R \tag{1}$$

where *MSL* is the mean sea level, η_A is the deterministic astronomical tide, η_{NTR} is the nontidal residual, and *R* is the wave runup [*Ruggiero et al.*, 2001] (Figure 2). Using equation (1), "observational" TWLs are derived by combining runup computed using both wave buoy data and estimates of beach slope with water levels from tide gauge measurements. In order to encompass as much of the range of variability as possible in the combination of components that drive extreme TWL events, a continuous, long record is preferable. To develop a TWL time series relevant to the northern Oregon coast, we obtained hourly water level data from the NOAA operated South Beach (SB) tide gauge station 9435380 (http://tidesandcurrents.noaa.gov/), located in Yaquina Bay, Oregon (Figure 1 and Table 1). The SB tide gauge record covers the time period of 1967–2012, and is the longest, most continuous record of water levels for the north-central Oregon coast. The raw data were adjusted for benchmark subsidence following the approach of *Burgette et al.* [2009].

The water level data extracted from the tide gauge consist of three of the components of the total water level, the MSL, η_A, and η_{NTR}. The MSL is the average sea level with respect to some datum, taken here to be the orthometric land-based datum NAVD88. The η_A is deterministic and can be computed using the station's harmonic constituents, while the η_{NTR} is defined as any elevation change in the water level not related to the deterministic tide. This can include low-frequency components like water level variability due to water temperature and the geostrophic effects of currents (e.g., the seasonal signal or monthly mean sea level anomalies) and/or high-frequency components due to the presence of winds and low atmospheric pressure (e.g., storm surge) [*Komar and Enfield*, 1987]. While the η_{NTR} is traditionally defined as the
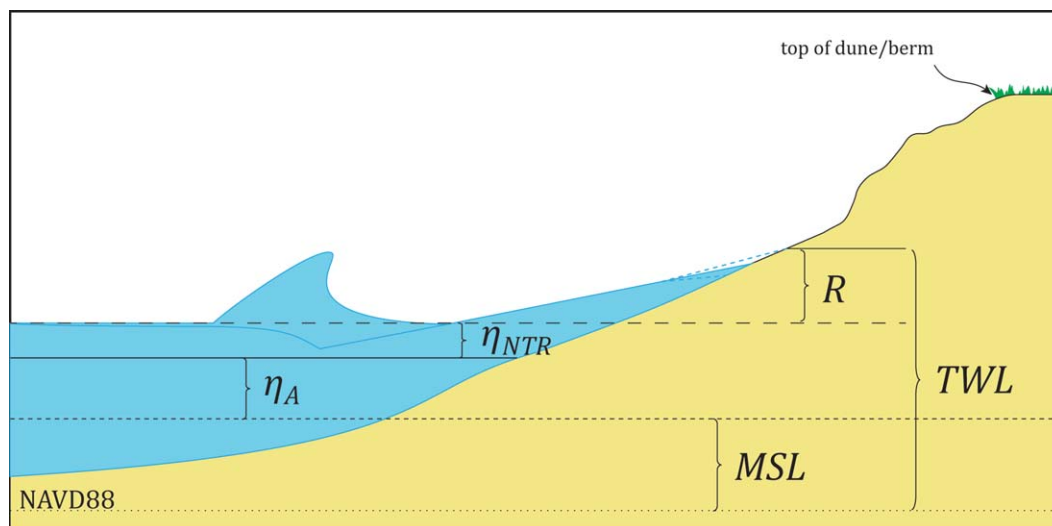
Figure 2. Definition sketch of total water levels (TWL) on a sandy, dune-backed beach. *MSL* is the mean sea level, (η_A) is the predicted astronomical tide, (η_{NTR}) is the nontidal residual and (*R*) is the wave-induced change in water level, wave runup. Dune erosion occurs when the TWL, relative to a datum such as the land-based NAVD88 datum, exceeds the elevation of the dune toe, and overtopping/flooding occurs when the TWL exceeds the elevation of the dune crest (modified from *Ruggiero et al.* [2001]).

difference between the measured tide and the predicted astronomical tide, η_{NTRs} produced through simple subtraction can be corrupted by timing errors or datum shifts [*Pugh*, 1987; *Haigh et al.*, 2013]. While these errors can be insignificant when the η_{NTR} is large, they can have greater influence on η_{NTR} estimates along coastlines with relatively modest η_{NTRs}, such as along the Oregon coastline where η_{NTRs} are rarely greater than 1 m [*Allan et al.*, 2011]. To more accurately extract the η_{NTRs}, 2 year blocks of the water level time series were transformed into the frequency domain and following the spectral methods of *Bromirski et al.* [2003], tide bands were removed and replaced with amplitude and phase estimates consistent with the concurrent nontide continuum. The result is a η_{NTR} time series that excludes energy at tidal frequencies and preserves seasonal oscillations in the water level.

The wave-induced component of TWLs, wave runup, is a combination of the maximum setup at the shoreline [e.g., *Longuet-Higgins and Stewart*, 1963, 1964; *Raubenheimer et al.*, 2001], and swash, the time-varying oscillations about the setup including both incident and infragravity motions. Wave runup is often empirically related to the deep water wave height, wave length, and the local beach slope [e.g., *Holman and Sallenger*, 1986; *Ruggiero et al.*, 2001], making it a highly site-specific computation. Here we use the empirical relation of *Stockdon et al.* [2006] for $R_{2\%}$, corresponding to the 2% exceedance percentile of extreme runup maxima on sandy beaches and parameterized by

$$R_{2\%} = 1.1 \left\{ 0.35 \beta_f (H_0 L_0)^{1/2} + \frac{\left[H_0 L_0 \left(0.563 \beta_f^2 + 0.004 \right) \right]^{1/2}}{2} \right\} \tag{2}$$

where β_f is the beach slope, H_0 is the deep water SWH, and L_0 is the deep water wave length (where $L_0 = gT_P^2 / 2\pi$, T_P is the peak wave period, and g is the acceleration due to gravity).

Buoys representative of northern Oregon include the deep water National Data Buoy Center (NDBC) (http://www.ndbc.noaa.gov/) buoy 46005, approximately 500 km from the coast, shelf-edge buoy NDBC 46089, approximately 150 km from the coast, and NDBC buoy 46029, 40 km from the Columbia River mouth (Figure 1 and Table 1). NDBC 46089 was chosen as the priority buoy for developing the combined time series due to its location, relatively close to the coast but in deep enough water such that the

Table 1. Wave Climate and Tide Gauge Data Sources

Name	ID	Source	Data Range	Depth
Wave Data				
Tillamook	46089	NDBC	Nov 2004–ongoing	2289 m
Columbia River Bar	46029	NDBC	Mar 1984–ongoing	144.8 m
Washington	46005	NDBC	Sep 1976–Jul 2012	2981 m
WIS Station	81048	USACE	Jan 1981–Jan 2011	N/A
Tide Data				
South Beach (SB)	9435380	NOAA	Feb 1967–ongoing	

data are not affected by shoaling and refraction processes. Since NDBC buoy 46089 has a modest record length (installed in 2004), other buoys in the region were used to complete the time series. Following the approach of *Allan et al.* [2012], we apply simple empirical transformations to the cumulative distribution functions of the wave climates of each individual buoy such that the transformed climates are representative of the climate at NDBC 46089. Remaining gaps in the record are filled with wave hindcast data obtained from the U.S. Army Corps of Engineers (USACE) Wave Information Studies (WIS), Station 81048 (http://wis.usace.army.mil/). Combining these transformed records, we create a nearly continuous 32 year hourly time series of waves (1980–2012) from which runup is calculated using estimates of SWH, T_p, and β_f extracted from lidar data (equation (2)). Runup is then combined with the tide gauge time series (accounting for wave propagation times from the shelf edge to the coast) and an almost continuous hourly record of "observational" TWLs is developed.

2.2. Sallenger's [2000] Storm Impact Scale

The exposure of the Rockaway, Oregon littoral cell to erosion and flood hazards can be assessed using the storm impact scaling approach of *Sallenger* [2000], which compares TWLs to the elevation of backshore morphology. Alongshore varying morphodynamic parameters such as dune crest, dune toe, and beach slope (the average slope between the horizontal location of mean high water (MHW) and the dune toe), were derived from high-resolution lidar data collected in September 2002 [*NOAA Coastal Services Center*, 2002]. Automated techniques first developed by *Plant et al.* [2002] and *Stockdon et al.* [2009] for the southeast U.S. coast were adapted by *Mull and Ruggiero* [2014] for the U.S. Pacific Northwest (PNW) coast and were used to extract these morphodynamic parameters at a 10 m resolution in the alongshore (Figure 3, plots 2 and 3).

Because our record is developed based on the deep water wave climate of the PNW (representative of the location of NDBC buoy 46089), it is necessary to propagate the waves toward the nearshore over the region's bathymetry. Numerically transforming waves for a number of time series would be prohibitively computationally expensive. Therefore, lookup tables (conceptually similar to the radial basis functions of *Gouldby et al.* [2014]) were developed to relate offshore (deep water) triplets of SWH, T_p, and mean wave direction (MWD) to their nearshore (~20 m water depth) equivalents in an efficient manner. The wave climatology was then discretized into 1738 representative wave conditions which were transformed to the nearshore over nested grids with 3′ to 30″ resolutions [*García-Medina et al.*, 2013] using stationary model runs of SWAN [*Booij et al.*, 1999]. Waves were transformed with a 100 m alongshore resolution to the 20 m contour (or where significant wave breaking first occurs, SWH$=h\gamma$, where $\gamma=0.4$, h$=$depth). Any combination of a deep water triplet's nearshore equivalent can then be interpolated from the 1738 model runs at each 100 m location (Figure 3, plot 4). A comparison between transforming specific wave conditions from the offshore to the nearshore using SWAN and transforming those waves to the nearshore using the lookup tables suggests interpolation errors typically less than 5% for each triplet variable [*Allan et al.*, 2012]. The *Stockdon et al.* [2006] wave runup parameterization relies on the deep water equivalent SWH and T_p as inputs, so transformed waves were linearly back shoaled from the 20 m contour to deep water.

Once alongshore varying dune morphology and hydrodynamics are produced, the storm impact scale [*Sallenger*, 2000] is applied to assess coastal hazards in northern Oregon. To investigate erosional events that have a high probability of occurrence throughout a given year, i.e., chronic hazards, we assess the amount of time that the TWL is between the dune toe and dune crest (TWL > dune toe, TWL < dune crest) and develop a parameter referred to as impact days per year (IDPY) as a proxy for erosion [*Ruggiero et al.*, 2001; *Ruggiero*, 2013]. To assess extreme flooding potential along the coastline, we examine the extreme TWL return levels (e.g., the 100 year event, the storm-induced TWL that has a 1% chance of occurring in any given year), and the elevation of the dune crest to determine the percentage of coastline the extreme event has the potential to overtop. If the TWL is higher than the dune crest (TWL > dune crest), we use this as a proxy for flooding. Because flooding and erosion hazards are most severe during maximum storm-induced TWLs, we focus on the evaluation of the most extreme events.

2.3. Evaluating Extreme Total Water Levels

The peak-over threshold (POT) approach [*Davison and Smith*, 1990], where some high-threshold, u, is selected and all peaks over that threshold, i.e., threshold excesses, are evaluated over a length of time, is chosen to model extremes due to its ability to capture a larger extreme data set than block maxima or r-largest methods [*Madsen et al.*, 1997a, 1997b; *Méndez et al.*, 2006]. All threshold excesses are assumed to
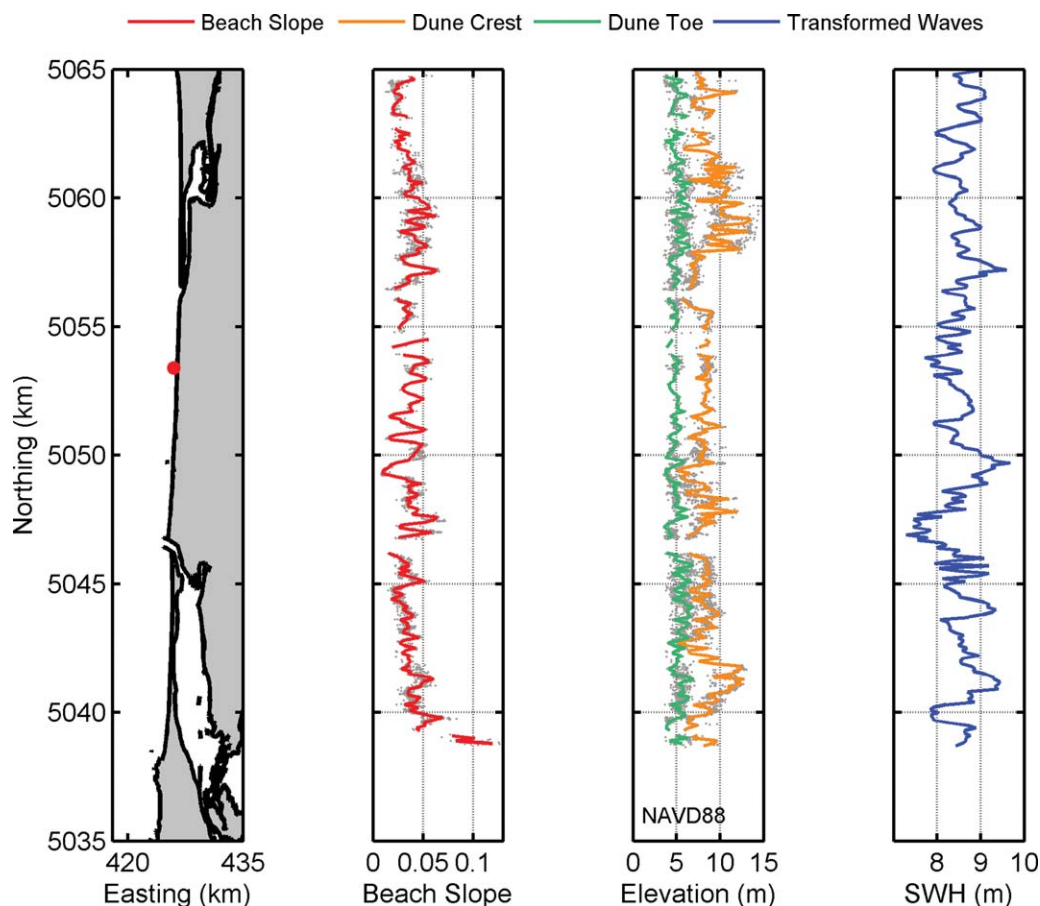
Figure 3. Geomorphic and hydrodynamic inputs for the application of *Sallenger*'s [2000] storm impact scale along the Rockaway, Oregon littoral cell. Data have been smoothed to a 100 m alongshore resolution. The most rightward plot is an example of a nearshore transformation from offshore NDBC 46089 to the 20 m contour for a significant wave height of 10 m with a peak period of 17 s. The red circle on the most leftward plot shows the location of the representative transect with $\beta_f \sim 0.04$ in the littoral cell.

be independent, identically distributed (iid) random variables, and are modeled using the Generalized Pareto Distribution (GPD),

$$G(y) = \begin{cases} 1 - \left(1 + \dfrac{\xi y}{\sigma}\right)^{-1/\xi} & \xi \neq 0 \\ 1 - \exp\left(-\dfrac{y}{\sigma}\right) & \xi = 0 \end{cases} \tag{3}$$

where y is a vector of threshold excesses, $(y = X - u)$, $\sigma > 0$ is the scale parameter, and ξ is the shape parameter. In order to combine the exceedences over a threshold, N, with the frequency of the exceedences, we use the GPD-Poisson model [*Smith*, 2001; *Katz et al.*, 2002; *Méndez et al.*, 2006], which assumes the number of exceedences from any given year follows a Poisson distribution with annual mean, vt, where v is the event rate per year and $t = 1$. This model relates to the Generalized Extreme Value (GEV) distribution for annual maxima [*Pickands*, 1975; *Coles*, 2001; *Smith*, 2001] by

$$\sigma = \psi + \xi(u - \mu), \qquad v = \left[1 + \xi \frac{(u - \mu)}{\psi}\right]^{-1/\xi} \tag{4}$$

where μ is the location parameter, $\psi > 0$ is the scale parameter, and the shape parameter, ξ, is common to both the GPD and GEV distribution. Parameters of both the GEV and GPD-Poisson distributions are estimated using maximum likelihood estimation (MLE), an optimization procedure which adopts the model that assigns the highest probability to the data through a likelihood function (see *Coles*, 2001, *Katz et al.*, 2002, or *Méndez et al.*, 2006 for more information).

2.3.1. Nonstationary Extreme Value Distributions

Since nonstationarity is inherent to many climatological processes [*Smith*, 2001; *Katz et al.*, 2002; *Milly et al.*, 2008; *Menéndez et al.*, 2009], the parameters of the GPD-Poisson model can be allowed to vary through time. Because of the relationship between the models (equation (4)), the GEV then also inherits this time-dependence, and the parameters, μ, ψ, and ξ, can be modeled as nonstationary variables containing seasonal effects, long-term trends, and climatic influences, such as ENSO variability [*Katz et al.*, 2002; *Méndez et al.*, 2006, 2007, 2008]. Interannual climate variability can be included in the model through regional climate indices as covariates [e.g., *Méndez et al.*, 2006]. Climate indices represent an aggregate summary of the state of the climate system, often related to ENSO. The climate indices of focus in this study, the Pacific/North American Pattern (PNA), the Southern Oscillation Index (SOI), and the Multivariate ENSO Index (MEI), are relevant to the northern hemisphere [*Stenseth et al.*, 2003] and previous studies have significantly related them to SWHs (PNA and SOI) [e.g., *Allan and Komar*, 2000; *Méndez et al.*, 2006], and sea levels (SOI and MEI) [e.g., *Méndez et al.*, 2007; *Komar et al.*, 2011]. For simplicity, here we only model the location parameter, $\mu(t)$, as a function of time, however, including nonstationarity in the other parameters is relatively straightforward [*Katz et al.*, 2002; *Méndez et al.*, 2007; *Menéndez et al.*, 2009].

2.3.2. Extreme Value Model Selection

To investigate model fits involving different arrangements of multiple parameters, we utilize a combination of information criteria, diagnostic plots, and likelihood ratio tests. The Akaike Information Criteria (AIC) [*Akaike*, 1974],

$$AIC = -2\hat{l}(p) + 2(p) \tag{5}$$

where p is the number of parameters in the model, and $\hat{l}(p)$ is the maximum of the log likelihood resulting from the model, is used to compare the quality of the goodness of fit and the complexity (number of parameters) of each model. The smaller the AIC, the better the model fit. However, the AIC does not decipher if all of the candidate models fit poorly. In order to test the fit of the candidate models, quantile-quantile (QQ) and probability (PP) plots are used for assessing how closely two data sets agree. In general, if the observed data follow the chosen distribution fit, they will fall onto a straight (one-to-one) line in a PP or QQ plot. Finally, to objectively determine which of the many potential models present the best fit to data, we use the likelihood ratio test [*McCullagh and Nelder*, 1989],

$$\{l_1(M_1) - l_0(M_0)\} > \frac{1}{2}\chi^2_{k,1-\alpha} \tag{6}$$

where $l_1(M_1)$ and $l_0(M_0)$ are the maximized log likelihood functions under nested models M_1 and M_0, respectively, and $\chi^2_{k,1-\alpha}$ is the $1-\alpha$ quantile of the χ^2 distribution with k degrees of freedom. Large values of this statistic indicate nested model M_1 explains substantially more of the variation then M_0, at the α level of significance.

2.3.3. Approaches for Estimating Return Level Events

The observational record approach combines, via equation (1), the measured water levels and computed wave runup into an hourly "observational" TWL time series which is then transformed into iid events by "declustering" (see section 2.4.1). The iid time series is then fit to extreme value distributions to determine the return level events of interest. To calculate a 100 year return level, even if the record does not exceed 100 years in length, the independent TWL record is fit to both stationary or nonstationary GPD-Poisson distributions and then the return level estimates, $\hat{y}_q(t)$, for the return period, $1/q$, are extracted using

$$\hat{y}_q(t) = \begin{cases} \hat{\mu}(t) - \dfrac{\hat{\psi}(t)}{\hat{\xi}(t)}\left\{1 - [-\log(1-q)]^{-\hat{\xi}(t)}\right\} & \hat{\xi}(t) \neq 0 \\[2ex] \hat{\mu}(t) - \hat{\psi}(t)\log[-\log(1-q)] & \hat{\xi}(t) = 0 \end{cases} \tag{7}$$

where $0 < q < 1$. Confidence intervals are obtained using the delta method [*Coles*, 2001], which uses the asymptotic normality property of maximum likelihood estimates.

We develop a full simulation method, described in detail in section 2.4 below, to model extreme TWL events not necessarily present in the extreme "observational" record, but physically capable of occurring. In order

to address the random co-occurrence of extreme events, we simulate daily synthetic records of arbitrary length of each of the main components of TWLs including SWH, T_p, η_{NTR}, and η_A. We also create synthetic records of mean wave direction (MWD), for modeling wave propagation to the nearshore, and of the selected climate indices to represent alternative climatic realizations. Return levels derived from this full simulation approach are empirically extracted directly from the synthetic data, using the "count back" method [*Hawkes et al.*, 2002; *Goring et al.*, 2010] and confidence intervals are estimated using bootstrapping techniques [*Efron and Tibshirani*, 1993; *Davison and Hinkley*, 1997].

2.4. Total Water Level Component Distribution Modeling

Below we outline how we model the individual components ultimately included in the TWL-FSM. Modifying the approach of *Callaghan et al.* [2008], we (1) fit independent extreme SWH and η_{NTR} events to a time-dependent GPD-Poisson model, (2) fit dependency distributions between the extreme SWHs and η_{NTRs}, (3) fit the conditional dependency between SWH and T_p, (4) determine an appropriate distribution fit to model MWD and climate indices, (5) determine an appropriate distribution fit to model the deterministic tide that occurs during the daily maximum TWL, and (6) simulate the wave climate, water levels, and ultimately the TWLs on beaches, using the prescribed distributions.

2.4.1. Fit Extreme SWH and η_{NTR} to Time-Dependent GPD-Poisson Models

In order to ensure the independence of large SWH and η_{NTR} events, we "decluster" storm events by choosing the maximum SWH and η_{NTR} event every 3 days [*Méndez et al.*, 2006; *Ruggiero et al.*, 2010], the approximate time scale of northeast Pacific extratropical storms. Following *Ruggiero et al.* [2010], thresholds for POT modeling were identified by selecting an average of five extreme events per year over the length of each record. We then fit the independent SWHs and η_{NTRs} over threshold to a variety of time-dependent GPD-Poisson distributions and select the model most representative of the distribution of each extreme time series.

2.4.2. Fit Dependency Distributions Between Extreme SWHs and η_{NTRs}

Modeling multivariate extremes adds a level of complexity compared to univariate modeling due to the interrelated nature of many processes, e.g., low-pressure atmospheric systems produce both storm surge and above average SWHs. In order to account for any dependency between SWH and η_{NTR}, we first convert the approximate marginal distributions of both physical variables using the transformation [*Coles*, 2001; *Callaghan et al.*, 2008],

$$x = \begin{cases} -\left(\log \left\{ 1 - v(t) \left[1 + \xi(t) \dfrac{X-u}{\sigma(t)} \right]^{-1/\xi(t)} \right\} \right)^{-1} & \hat{\xi}(t) \neq 0 \\[3mm] -\left(\log \left\{ 1 - v(t) \exp \left(\dfrac{X-u}{\sigma(t)} \right) \right\} \right)^{-1} & \hat{\xi}(t) = 0 \end{cases} \tag{8}$$

where X are the threshold excesses and $v(t)$, the probability of an individual observation to exceed the threshold, u, is calculated using equation (4). The transformed variable, x, has a distribution function with margins that are approximately standard Fréchet when $X > u$ [*Coles*, 2001]. This transformation of X is used for both SWH and η_{NTR} and allows for the comparison of the two variables in a consistent scale, where the distribution's dependence characteristics are well understood. Following *Callaghan et al.* [2008], we use the logistics model [*Tawn*, 1988] to model the dependency between SWH and η_{NTR},

$$P\{X \leq x, Y \leq y\} = F(x,y) = e^{-\left[x^{-\alpha^{-1}} + y^{-\alpha^{-1}} \right]^{\alpha}} \tag{9}$$

where x and y are the rescaled Fréchet variates and α is the measure of dependence between them. When $\alpha = 0$, x, and y are perfectly dependent variables, while $\alpha = 1$ corresponds to x and y being independent variables. The dependency parameter, α, is estimated by maximizing the log likelihood of this function, which is censored when a bivariate pair exceeds a threshold in just one of its components [see *Coles*, 2001; *Callaghan et al.*, 2008]. We assume that the dependency between SWH and η_{NTR} is stationary.

2.4.3. Fit Conditional Dependency Between SWH and T_p

T_p is conditionally related to SWH due to physical mechanisms, such as wave steepness, (SWH/L), that restricts the possible range of T_p for a given SWH. *Callaghan et al.* [2008] modeled T_p variability with a log-normal distribution described by three parameters dependent on SWH. For the PNW data set, we find better

model fits when the T_p variability is modeled using a normal distribution with the mean, μ_T, and standard deviation, σ_T, as a function of SWH as follows,

$$(\mu_T, \sigma_T) = \left(a(SWH)^b, \left(\frac{2c}{SWH} \right)^{1/2} \right) \tag{10}$$

where a, b, and c are fitted parameters.

2.4.4. Determine the Distribution Fit for MWD and Climate Indices

In order to incorporate seasonality into parameters not modeled using extreme value distributions, we investigate their known monthly empirical distributions. Since the monthly distributions of MWD failed to quantitatively fit any standard known distributions, these distribution fits are modeled empirically from the observed data.

If the most representative GPD-Poisson model fit for SWH or η_{NTR} includes a proxy for interannual climate variability, monthly distributions of the selected climate indices are modeled using their respective monthly empirical distributions. This allows for random realizations of ENSO and other low-frequency climate variability to influence the simulated extreme events in patterns modeled from the recorded climate indices.

2.4.5. Determine the Distribution Fit for Tide During the Daily Maximum TWL

The maximum TWL does not always occur during the daily maximum high tide, such that choosing to consistently simulate the daily maximum tide would artificially inflate estimates of TWLs. To avoid contriving conservatism, we investigate the percentage of time that the daily maximum "observational" TWL coincides with the maximum daily tide. After accounting for these instances, we develop an approach for appropriately simulating the differences between the daily maximum tide and the tide occurring during the daily maximum TWL. These differences are separated into four exponentially distributed elevation bins, such that each bin relates to a group of elevations of the daily maximum tide. Random sampling of the exponential distribution from each bin produces a value to subtract from the daily maximum tide, ensuring extreme TWL occurrence over an accurate range of tide levels.

2.4.6. Simulating Total Water Levels

Synthetic time series are simulated for each component of the TWL beginning at time t_0 using Monte Carlo simulation techniques. In order to simulate in a Monte Carlo sense, random numbers are generated from a uniform distribution based on each TWL component's prescribed cumulative distribution function (CDF) (Table 2). Therefore, given any cumulative probability distribution function, $F(x) = P\{X < x\}$, we can transform a uniform distribution, $U(0, 1)$, to $F(x)$ by solving $F(x) = P\{X < x\} = A$, where $A \sim U(0, 1)$ (see Figure 4, top). For SWH and η_{NTR}, we transform the random number estimate, A, to the known distribution that the SWHs and η_{NTRs} have previously been transformed to, the Fréchet distribution. Based on the probability of occurrence of the transformed value, the estimate is transformed back to the physical scale via the GPD-Poisson or the fitted monthly distribution, dependent on the variable's threshold (see Figure 4, bottom).

Following methods from *Callaghan et al.* [2008], we use the two-step Gibbs sampling technique [*Geman and Geman*, 1984]. In order to incorporate the standard errors of the GPD-Poisson parameter estimates into the simulation, we sample parameter estimates from a Gaussian distribution where the best fit model's parameters are the mean and the standard errors are the approximate standard deviations.

Table 2. Sampling Distributions for Simulating Each TWL Component[a]

Component	Nonextreme	Extreme
SWH (m)	Monthly lognormal distribution	Nonstationary GPD-Poisson
MWD (°)	Monthly empirical distribution	
T_p (s)	Normal distribution conditionally dependent on SWH	
η_{NTR} (m)	Monthly logistic distribution	Nonstationary GPD-Poisson
η_{A-TWL} (m)	60% daily maximum tide; 40% slightly less	
Climate indices	Monthly empirical distribution	

[a]Distributions selected for simulating the TWL component parameters are discussed in section 2.4.

2.4.6.1. Simulation Procedure

1. Randomly sample from the monthly empirical CDF of each climate index. If two indices are linearly correlated, this correlation is reproduced in the simulations for that month.

2. Simulate time-dependent SWH and η_{NTR} following steps 1 and 2 (a, b, c, and e) in section 3.1.7 of *Callaghan et al.* [2008]. For picks lower than threshold values, probability distributions for random sampling are
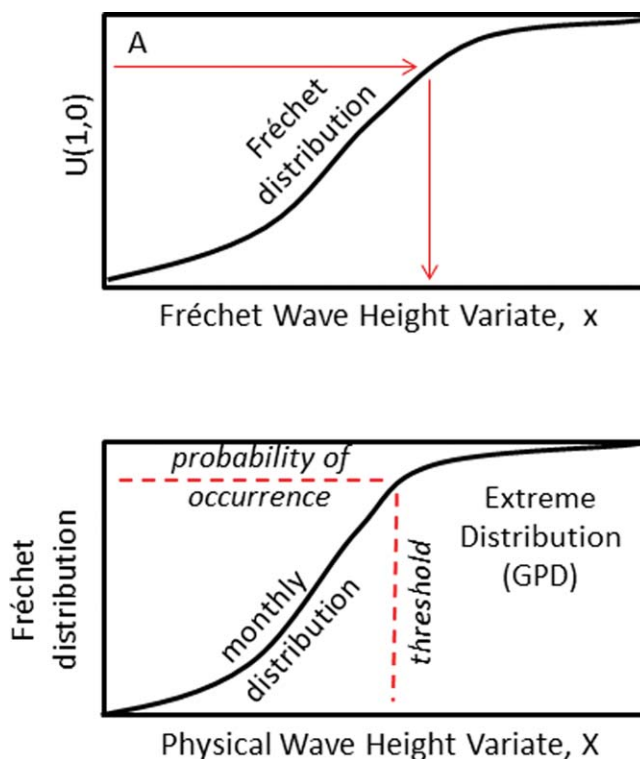
Figure 4. Schematic of the simulation process across different distribution scales. (top) Transformation of a uniform random variate, A, to a known distribution. In this case, the known distribution is the Fréchet distribution. (bottom) The physical variate is then transformed out of Fréchet space based on the probability of occurrence, v, of x determined by either the fitted monthly distribution or GPD-Poisson distribution if below or above threshold, respectively (modified from *Callaghan et al.* [2008]).

defined by (1) lognormal distribution fits to the monthly empirical distributions for SWH and (2) logistic distribution fits to the monthly empirical distributions for η_{NTR}. In order to incorporate the standard error in parameter estimation for distribution fits, the parameters estimated for each distribution (GPD, logistic, and lognormal) are randomly simulated.

3. T_p is simulated from the normal distribution (equation (10)). First, σ_T and μ_T are determined based on the randomly generated SWH, then T_p estimates are randomly selected from the derived normal distribution.

4. MWD is randomly simulated from the monthly empirical cumulative distribution function. If MWD is linearly correlated with SWH, this correlation is reproduced in the simulations.

5. In order to simulate the tide, the 32 year deterministic tide time series is repeated such that we are simulating "modern day" extremes and not including longer-term tide cycles in our time series. This is to ensure an accurate comparison between simulated and "observational" extreme TWLs. First, the daily maximum tide for every day is selected from the repeated tide time series. In this case, the maximum daily TWL occurs during the maximum daily tide approximately 60% of the time. Therefore, for 40% of the data, the tidal estimate must be less than the maximum daily tide. This is achieved by selecting a random day in time from the daily maximum time series. The maximum tidal elevation for that day fits into one of the four previously determined elevation bins, which correspond to an exponential fit representing the differences between the tide during the daily maximum TWL and the maximum daily tide. A random estimate is sampled from the exponential, and this value is subtracted from the maximum daily tide.

These steps are repeated for approximately 186,270 iterations, creating synthetic daily maxima TWL records with lengths of 510 years. The first 10 years of data are wasted to ensure the simulation converges to a Markov Chain. To optimize the number of simulations necessary to robustly estimate extreme TWLs, the mean of the 50 and 100 years SWH and η_{NTR} return levels are examined for stability. This produces multiple, synthetic, TWL components representing different realizations of the daily "observational" record.

3. Results

We first characterize the climatologies of the measured wave, water level, and computed hourly TWL records at a representative transect in the Rockaway littoral cell. Next, we describe the selected nonstationary extreme value models characterizing the extreme, independent SWHs and η_{NTRs}. Then, we demonstrate that the synthetic records accurately represent the daily "observed" TWL components and compare TWL return level events. Last, we compare the "observed" and simulated alongshore variable impact days per
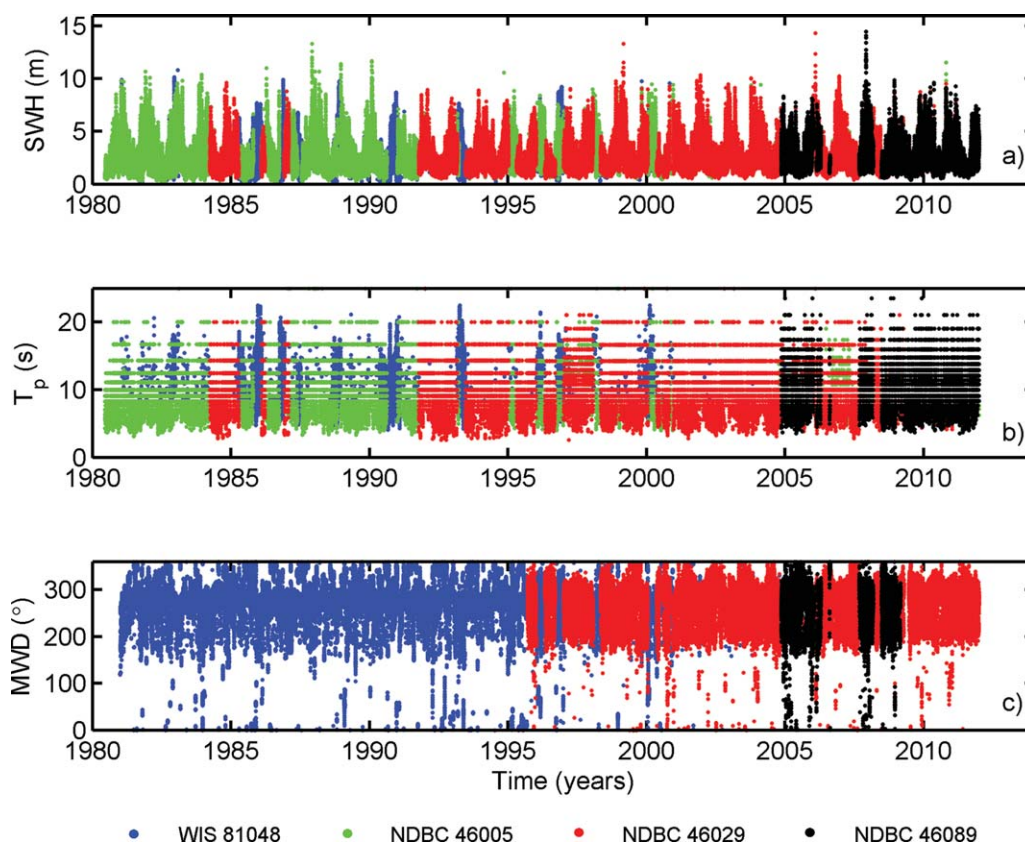
Figure 5. Combined wave buoy and hindcast data transformed to represent NDBC 46089. The different colors represent wave data from different sources where NDBC buoy 46089 is represented by black, NDBC buoy 46029 is represented by red, NDBC buoy 46005 is represented by green, and WIS hindcast 81048 is represented by blue. See Figure 1 for NDBC buoy and WIS hindcast locations.

year (IDPY) and overtopping from extreme return levels for the Rockaway, Oregon littoral cell in the context of exposure to extreme events.

3.1. TWL Time Series

Continuous hourly time series for all TWL components were generated for northern Oregon. Time series representing NDBC buoy 46089's wave climate produced an approximately 32 year record with 99.3%, 99.3%, and 95.1% coverage of SWH, T_P, and MWD, respectively (Figure 5). In this region, the tide is mixed and predominantly semidiurnal. Spectral removal of the tide bands results in a η_{NTR} time series that excludes tidal signals, preserves seasonal oscillations in the water level (Figure 6), and covers 99.1% of the 32 year record. Alongshore varying beach slopes (β_f) were then combined with the transformed wave climate data using equation (2), to produce alongshore varying $R_{2\%}$ estimates, that are 95.1% complete. Here we examine a representative transect near the center of the Rockaway Beach, Oregon subcell with a foreshore beach slope of approximately 0.04. Combining all components, produces an "observational" hourly TWL time series that is 94.3% complete between 1980 and 2012 (Figure 6).

Significant seasonality exists in both the wave and water level components comprising the TWLs at the representative transect. SWHs are on average 3.1 m in the winter, with an average T_p of 11.8 s. These values decrease to 1.9 m and 9.7 s in the summer for SWH and T_p, respectively. η_{NTRs} have similar seasonal fluctuations and vary about 24 cm between summer (lower) and winter (higher). Much like SWH and η_{NTRs}, TWLs are also higher in the winter. The largest monthly averaged TWL is 2.6 m with a seasonal range of approximately 1 m (Figure 7).

The maximum TWL event in the hourly record is 6.9 m, relative to NAVD88. This event was produced by the combination of a 2.33 m tide (probability of exceedance ~4.0%), a 0.48 m η_{NTR} (1.5%), a 11.5 m SWH (0.01%), and a 20 s T_p (0.15%) that occurred on 2 December 1987. $R_{2\%}$ during this event (at the
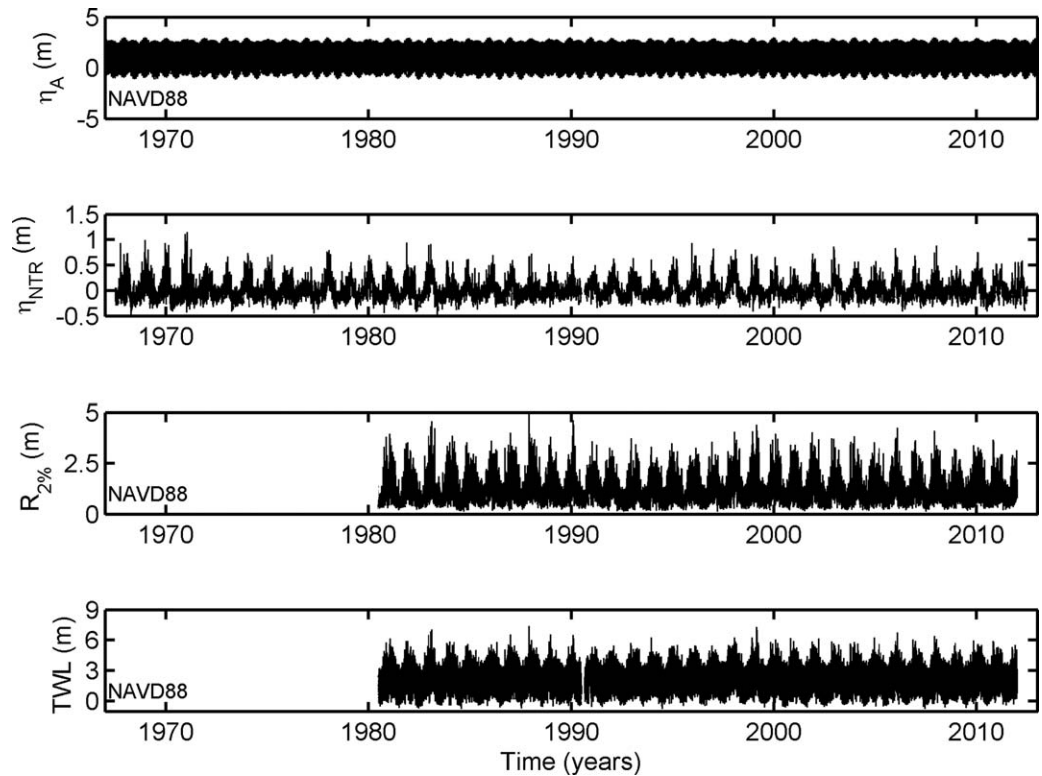
Figure 6. Hourly "observational" tide (η_A), nontidal residual (η_{NTR}), wave runup ($R_{2\%}$), and computed total water level (TWL) time series for northern Oregon over 1980–2012, relative to NAVD88.

representative transect with β_f, =0.04) was 4.09 m (0.002%)), and therefore contributed approximately 60% of the TWL (Figure 8). In more than half of the ~150 events included in extreme value analysis (~5 events per year), wave-induced water levels accounted for >50% of the TWL signal.

Note that the most extreme TWL was not produced by the largest event on record for any of the individual components at this transect. If the largest event corresponding to each TWL component (SWH = 14.5 m, occurring on 3 December 2007, T_p = 20 s, the largest period conditionally dependent on a 14.5 m SWH in this region, η_A = 2.97 m occurring on 29 January 1983, and η_{NTR} = 0.95 m occurring on 15 November 1981) had coincided (a very improbable occurrence), the maximum TWL produced would be approximately 2 m higher than the largest "observed" at this transect.

3.2. Selected Extreme Value Models

Independent extreme SWHs and η_{NTRs} were fit to a variety of nonstationary extreme value models in order to find the model that best represents each component's variability over different time scales. Threshold values of 7.5 and 0.45 m, for SWH and η_{NTR}, respectively, were selected based on ensuring approximately five extreme events on average per year. Models were tested and compared considering long-term trends, seasonal cycles, and proxies for interannual climate variability. Ultimately, the model that explains the most variability in the extreme SWH is

$$\mu_{SWH}(t) = \beta_0 + \beta_1 \cos(2\pi t) + \beta_2 \sin(2\pi t) + \beta_3 \cos(4\pi t) + \beta_4 \sin(4\pi t) + \beta_{PNA} PNA(t) \tag{11}$$

while extreme η_{NTR} fit best to the model

$$\mu_{NTR}(t) = \beta_0 + \beta_1 \cos(2\pi t) + \beta_2 \sin(2\pi t) + \beta_{PNA} PNA(t) + \beta_{MEI} MEI(t) \tag{12}$$

where t is time in years, β_0 is a mean value, β_1, β_2 are coefficients corresponding to the annual cycle, β_3, β_4 are coefficients corresponding to the semiannual cycle, and β_{MEI}, β_{PNA} are linear coefficients corresponding to the PNA or MEI climate indices. The most representative model was selected by evaluating the AIC and comparing to other nested models using the likelihood ratio test as a measure of significance.
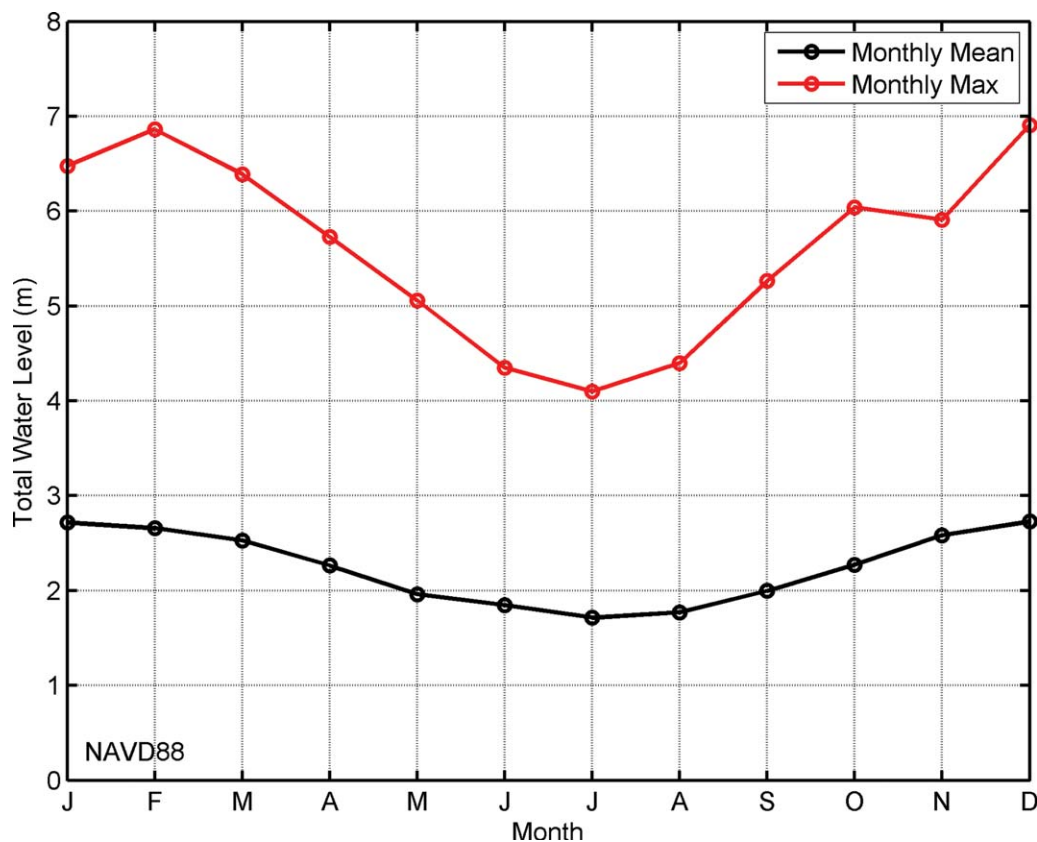
Figure 7. Representative TWL climatology (representative transect $\beta_f = 0.04$). The two lines indicate the monthly mean TWL (black) and the monthly maximum TWL (red) in respect to NAVD88.

Most of the variation in the SWH data is due to the seasonal cycle, modeled as two harmonics within the location parameter. The remaining variation is due to climatic variability represented by the PNA. The most representative model fit lowers the minimized negative log likelihood by 183 units as compared to the stationary model fit, statistically significant at the 0.000001 level. Compared to the next best nonstationary model fit, which does not include a climate index, the selected model is statistically significant at the 0.03 level. The estimated value of β_{PNA} in the selected model is 0.29, so that every unit increase in PNA results in an estimated increase of approximately 29 cm in SWH. For example, this means that for a particularly high PNA value of 2.5, occurring during the 1982/1983 El Niño, 0.7 m of extreme wave height variability can be related to the climate patterns the PNA represents.

The majority of the seasonal variation in the η_{NTR} can be represented by a single harmonic. The rest of the variation in the η_{NTR} is due to climate variability modeled by both the MEI and the PNA. This fit improves the minimized negative log likelihood by approximately 287 units, also statistically significant at the 0.000001 level when compared to the stationary model fit. Compared to the next best model fit, which represents climate variability described by only the MEI, the selected model is statistically significant at the 0.01 level. Every unit increase in the PNA and MEI results in approximately 1.9 cm and 3.2 cm of increased water levels, respectively. This attributes approximately 13 cm of water level elevation during strong El Niño years when the MEI index is close to a value of 3 and the PNA is near 2.

3.3. Full Simulation

To optimize the number of simulations necessary to robustly estimate extreme TWLs, the mean of the 50 (not shown) and 100 year SWH and η_{NTR} return levels are examined for stability. After 45 iterations, 100 year return levels stabilize around 0.99 and 14.6 m for η_{NTR} and SWH, respectively (Figure 9). We therefore choose to simulate 50 synthetic records of each TWL component as a representative
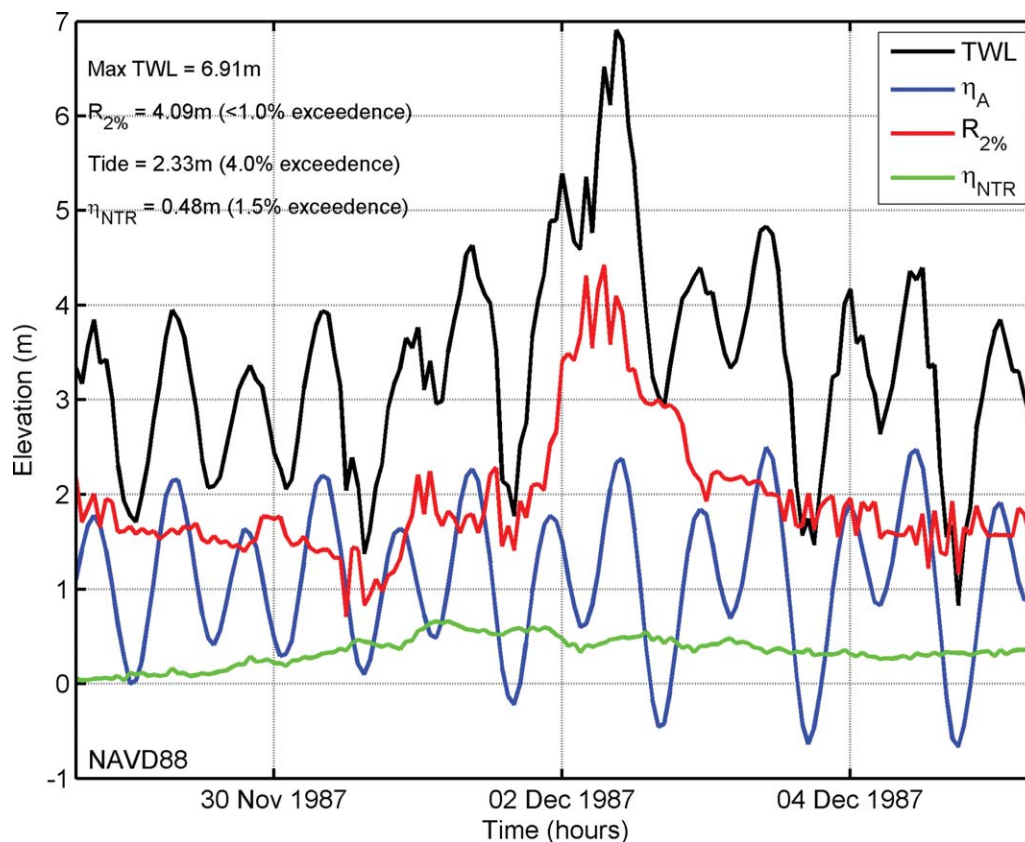
Figure 8. The individual components, $R_{2\%}$, tide, and η_{NTR} of the maximum "observational" total water level (TWL) on record, in respect to NAVD88. $R_{2\%}$ accounts for approximately 60% of this elevation.

sample size for return level estimation. Climate indices were linearly correlated for the months of January to April, and during these months, the simulations must account for this correlation. Cumulative distribution functions (CDFs) of simulated daily maxima for each wave climate parameter (SWH, T_p, MWD) compares well to the CDFs of the daily "observational" wave parameters (Figure 10). The main focus of this study is on the extreme events, which are represented in the tail of the CDF due to their low probability of occurrence. Similar to the comparison with the whole CDF, the tails of the simulated parameter CDFs and the tails of the daily "observed" CDFs also compare well (Figure 10 insets). This result confirms that the distribution of each wave climate parameter has been simulated appropriately. Because not all of the components are independent (e.g., SWH and η_{NTR}, SWH and T_p, MEI and PNA) scatterplots of TWL components are investigated to ensure an example simulation reproduces the relationship between dependent components (Figure 11). Careful consideration has been taken to model the dependency between SWH and η_{NTR}, and that the percentages of simulated data are represented well in each of the four quadrants ((1) $(H_S \leq u_{H_s}, \eta_{NTR} > u_{NTR})$, (2) $(H_S \leq u_{H_s}, \eta_{NTR} \leq u_{NTR})$, (3) $(H_S > u_{H_s}, \eta_{NTR} > u_{NTR})$, and (4) $(H_S > u_{H_s}, \eta_{NTR} \leq u_{NTR})$) (Figure 11). The difference in the percentage of the simulated and independent "observed" SWH and η_{NTR} over their respective thresholds is under 8%. We find similarly acceptable agreement for the joint distributions of SWH and T_p, SWH and MWD, and the correlation between the MEI and PNA indices (Figure 11).

CDFs of the $R_{2\%}$ and the simulated water level parameters, η_{NTR} and tide during the daily maximum TWL, also agree with the daily "observed" distributions used for model input (Figure 12). Again, since the tails of the CDFs of the individual simulated TWL components represent the tail end of the CDFs of the input data very well (Figure 12), any change in our eventual estimates of extreme TWLs will be primarily due to the synthetic data set capturing more combinations of the co-occurrence of large events. Last, we compare one example synthetic record to the daily "observational" time series for each TWL component. From this
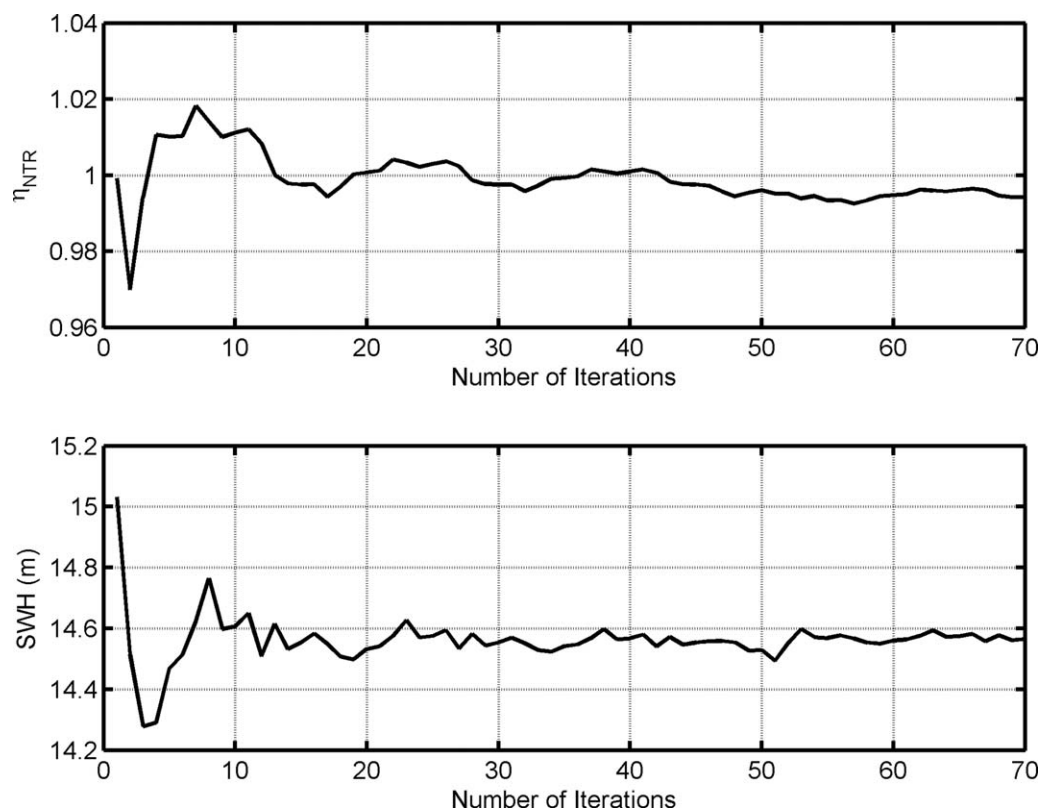
Figure 9. 100 year return level estimates for SWH and η_{NTR} by number of iterations, computed by averaging each additional simulation return level estimate. The number of simulations was selected based on the amount of runs necessary for this variable to become stable.

comparison, it is qualitatively clear the simulations of daily maxima adequately reproduce the seasonality inherent to the data set, as well as the interannual variability over a 32 year period (Figure 13).

3.4. Return Level Estimates

Return level estimates from the independent "observational" TWL record at the representative transect are extrapolated from the extreme value distribution fit ($u_{TWL} = 5.0$ m) using equation (7). At this location, the return level estimate of the 10 year event is 6.47 m (± 0.25, 95% confidence interval), while the 100 year event is 7.08 m (± 0.56, 95% confidence interval). In comparison, the average TWL return levels and corresponding 95% confidence intervals for the 10 and 100 year event across all 50 full simulation runs are 6.67 m (± 0.16, 95% confidence interval) and 7.37 m (± 0.26, 95% confidence interval), respectively (Figure 14 and Table 3). Extreme TWL return levels produced by the TWL-FSM are slightly larger than those extrapolated from the 32 year "observational" record with tighter confidence bounds. This suggests that, given sufficient time, the random superposition of TWL components can combine to produce extremes that are larger than those that occurred in the relatively short "observational" record.

3.5. Application for Evaluating Chronic and Extreme Coastal Hazards

Dune impact (TWL>dune toe, TWL<dune crest) from the alongshore varying TWLs computed from the nearshore-transformed daily "observational" record is highly variable across the littoral cell with an average of approximately 15 (standard deviation=23) impact days per year (IDPY). Results from the TWL-FSM show the alongshore average increases to 21 (standard deviation=29) IDPY (Figure 15). The average dune height along this littoral cell is 8.4 m, which limits how often this stretch of coast is overtopped during the year; however, simulations indicate the lowest lying elevations may overtop 1–9 times a year, while the daily "observational" record indicates less frequent overtopping. While highly variable across the littoral cell, an increase of impact and overtopping days per year implies more areas may be vulnerable to chronic erosion and flood hazards than the daily "observational" record suggests.
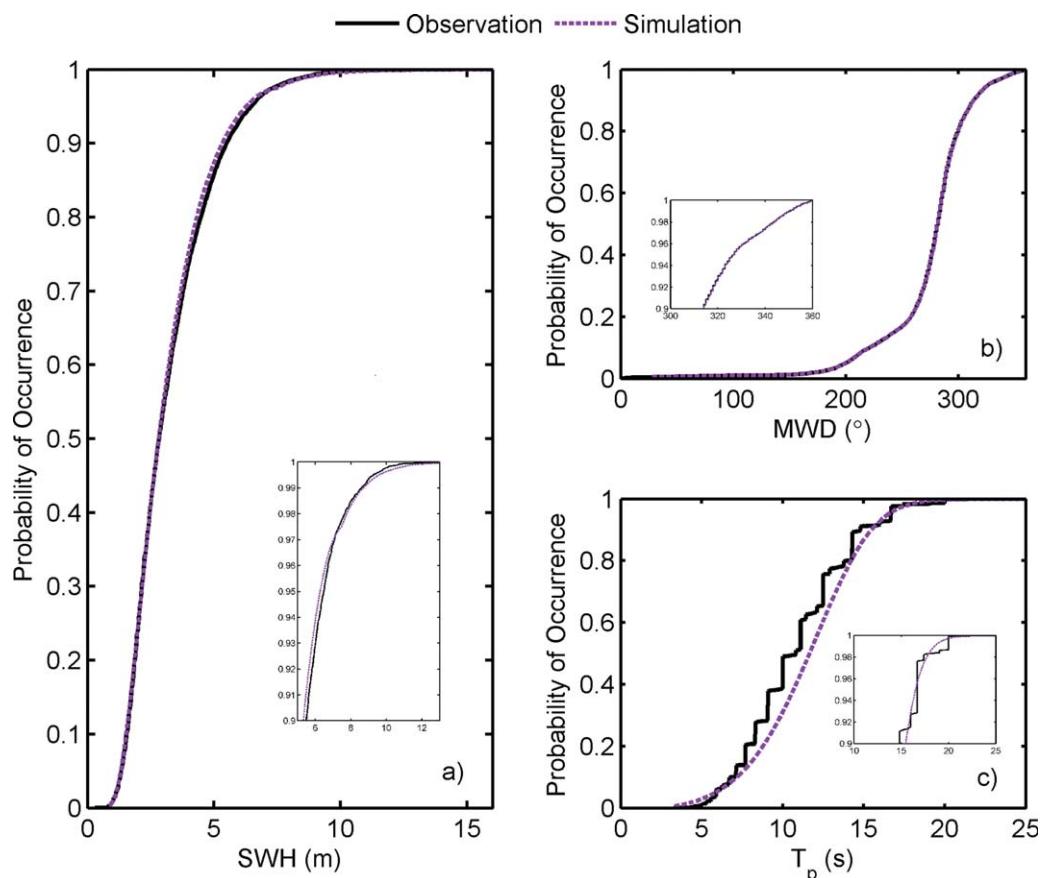
Figure 10. Cumulative distribution functions (CDF) comparing the simulated wave climate record (purple) to the daily "observational" record (black). (a) The significant wave height, (b) The mean wave direction, and (c) The peak period. Insets of tail behavior are included to show consistency in the extremes, the focus of this study.

We also compare the alongshore varying 100 year TWL return level produced by the nearshore-transformed "observational" record and the synthetic record to estimate extreme flooding potential along the Rockaway littoral cell. The extracted "observational" 100 year return level estimate overtops (TWL>dune crest) 17% of the coastline, while the mean 100 year event produced by the TWL-FSM results in 22% of the dunes overtopping (Figure 16). The maximum difference between the synthetic 100 year TWL return level estimates and the "observed" 100 year TWL return level estimates across all beach slopes in this littoral cell is just under 1.0 m, while the average difference is approximately 30 cm (Figure 17). Simulation return levels result in an increased percentage of overtopping and tighter confidence bounds on these events compared to the "observational" return levels.

4. Discussion

The addition of climate indices into the modeling of extreme SWH and η_{NTR} events allows for evaluation of the amount of variability that is due to large-scale climate patterns, e.g., ENSO. The PNA is a measure of the strength of the westerly winds and the position of the jet stream, both of which have a major influence on wave generation in the region [*Hasselmann et al.*, 1976]. Because the PNA is related to the position of storm tracks in the northeast Pacific, it could also influence episodic storm surge events driven by strong winds. The MEI quantifies ENSO variability over six variables, including sea level pressure, surface winds, and sea surface temperature. Since a η_{NTR} by definition includes water level changes due to a range of nontidal processes, the correlation we find with the MEI is intuitive. The simulation of the climate indices relating to extreme wave and water levels allows the TWL-FSM to represent large-scale climate patterns with a similar frequency of occurrence and similar monthly distributions to the historical records of the climate indices. The multiple realizations of the simulated climate indices not only properly represent the distributions of the
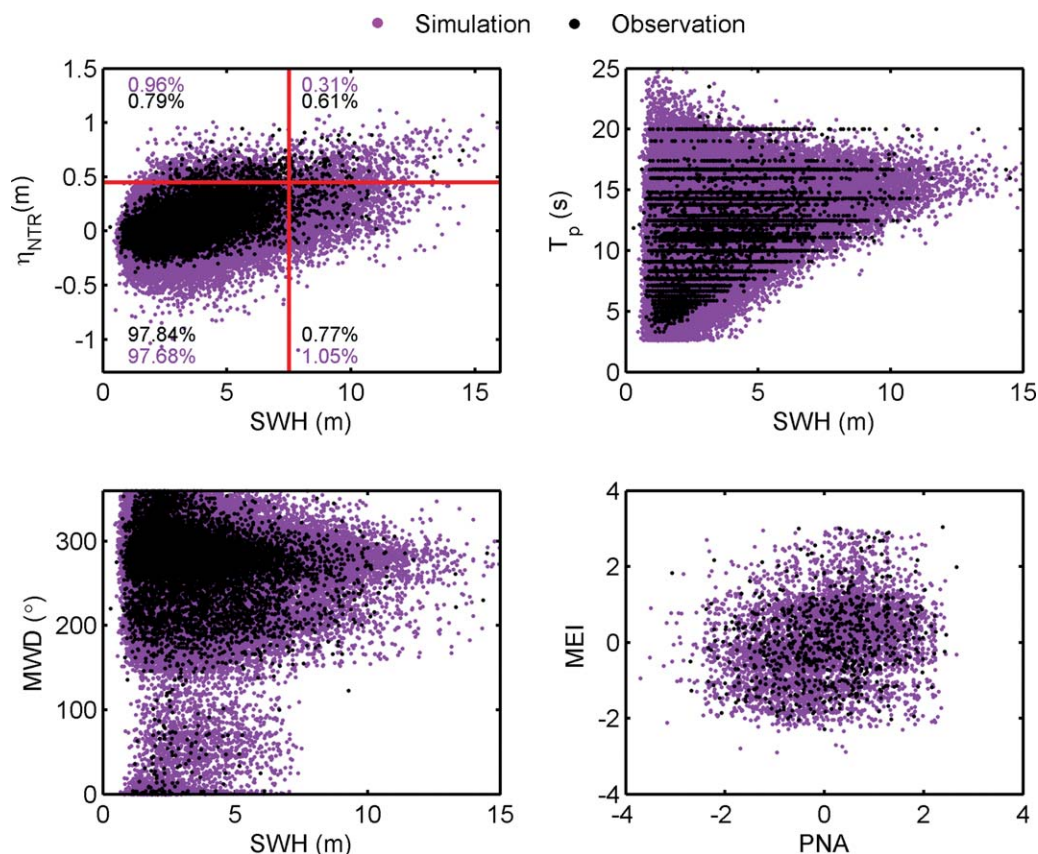
Figure 11. One example simulation (purple) compared to the daily "observational" record (black). (top left) The significant wave height (SWH) plotted against the nontidal residuals (η_{NTR}). (top right) The SWH plotted against the peak period (T_p). (bottom left) The SWH plotted against the mean wave direction (MWD). (bottom right) The MEI index plotted against the PNA index. Red lines on the top left plot indicate the respective thresholds for η_{NTR} and SWH.

historical records, but also permit randomness in the order of ENSO events driving interannual variability in extreme TWLs.

Generating synthetic records with a length of 500 years allows for the empirical extraction of return level events rather than an extrapolation from a model fit to a short record. If, however, we investigate the influence of fitting the extreme value distributions to 32 year segments of synthetic data (to be consistent with the length of our "observational" time series), the parameter estimates are within the standard error bounds of the input GPD-Poisson distribution fits and the return level estimates still converge on the empirically extracted return levels. Simulated extreme TWL return levels result in increased overtopping and tighter confidence bounds on these events compared to the "observational" return levels, further emphasizing the benefit of simulating different combinations of the TWL components. These findings suggest current application of a projected 100 year TWL event or the maximum water level on record as the extreme event estimate may not be sufficient for coastal hazard planning.

Our initial comparison between the "observed" and simulated extreme return level events described above (Figure 14 and Table 3) uses only a single representative cross-shore transect with a beach slope of approximately 0.04. Taking the alongshore variability into account for both the simulated and "observational" record results in 100 year TWL return levels that are on average, 30 cm higher, but can be as large as 90 cm higher than "observational" 100 year TWL return levels for various beach slopes across the littoral cell (Figure 17). Across the majority of the Rockaway littoral cell, an increase to the 100 year TWL return level of approximately 30 cm is not enough to overtop much more of the dune on this coastline (22% versus 17%). However, comparing the maximum simulated 100 year TWL return level event across all transects with the "observed" 100 year TWL return level increases the total overtopping to 30%, impacting 76% more of the coastline than the "observational" return levels project. The average 100 year event estimated by the TWL-FSM is rarely less
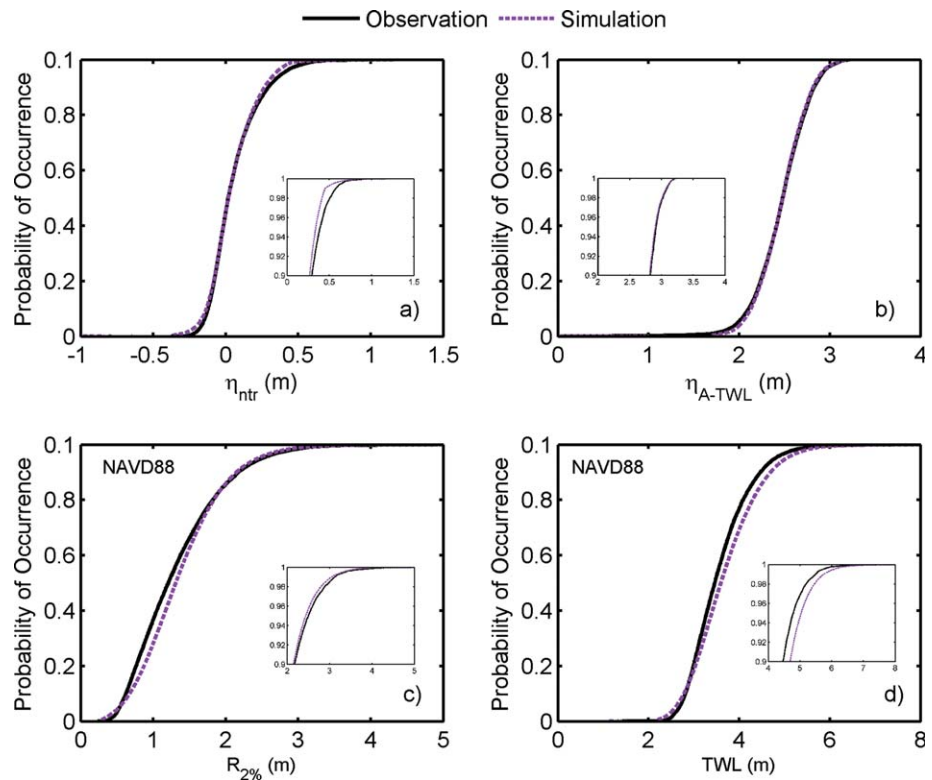
Figure 12. Cumulative distribution functions (CDF) comparing the TWL components from the simulated record (purple) to the daily "observational" record (black). (a) The nontidal residual (η_{NTR}), (b) the maximum tide during the TWL (η_{A-TWL}), (c) the runup ($R_{2\%}$), and (d) the total water level (TWL). Insets of the tail behavior are included to show consistency in the extremes.
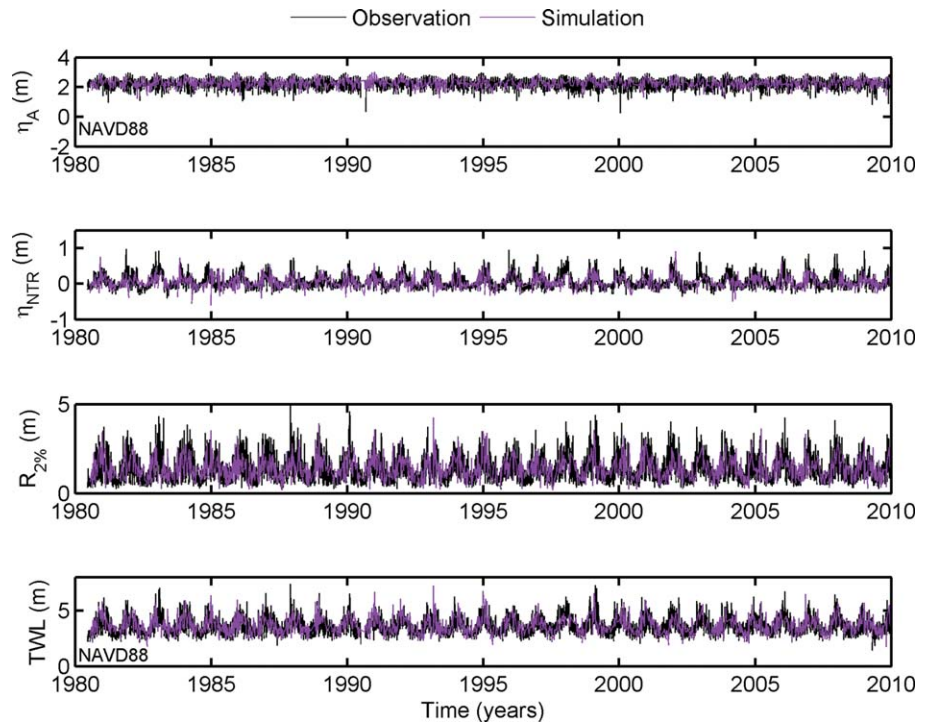

Figure 13. One sample synthetic record (purple) compared to the daily "observational" time series (black). Plotted are all the components of the TWL: tide during TWL (η_{A-TWL}), nontidal residual (η_{NTR}), and runup ($R_{2\%}$).
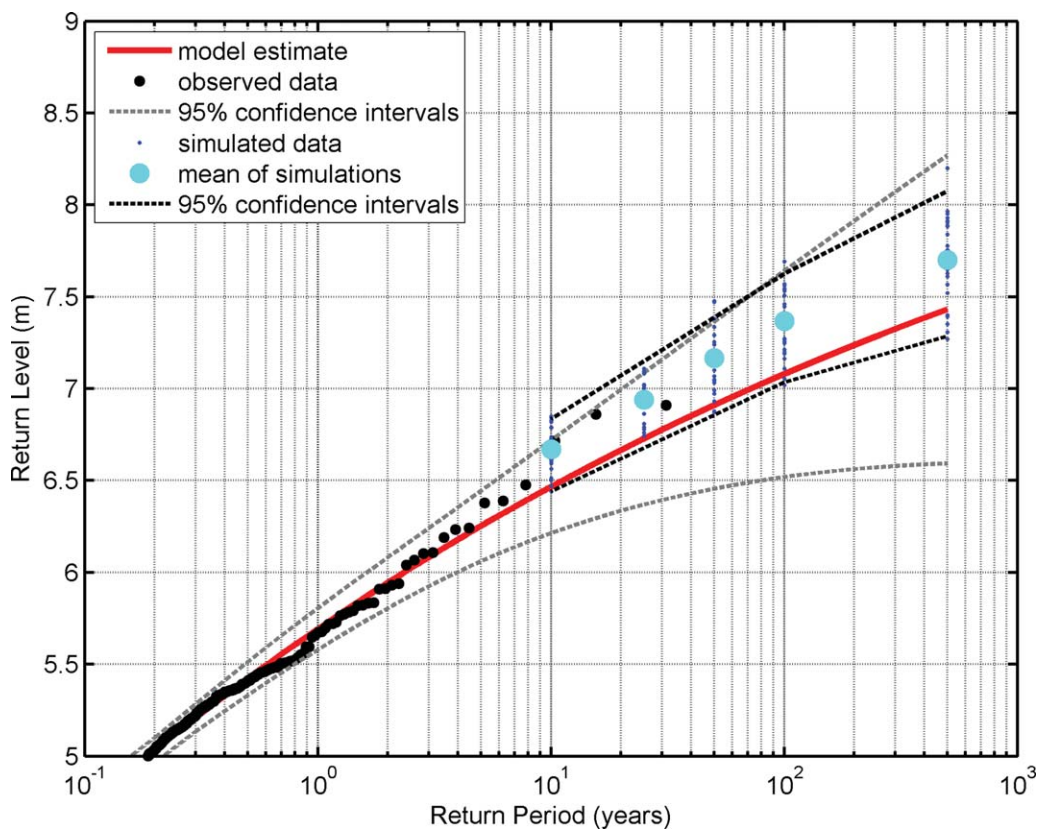
Figure 14. Comparison of total water level (TWL) return level estimates extrapolated from the independent "observational" record using extreme value theory and extracted from the TWL-FSM results. In this case, waves are shoaled to the nearshore then reverse shoaled to deep water before TWL computation. Black points are the independent "observational" TWL estimates, the red line is the best model fit, and the gray hashed lines represent the 95% confidence intervals on the model fit. Blue points are the TWL return levels from each of the 50 simulations, cyan points are the average return level from the 50 simulations, and black hashed lines are the bootstrapped 95% confidence intervals.

than the 100 year event estimated by the "observational" record, and the spread of the simulated 100 year return level show mostly positive differences between these two events (Figure 17). Therefore, across a range of hydrodynamic inputs and varying coastal morphology, the TWL-FSM indicates a potential for higher return level events than the "observational" record estimates.

While the simulated synthetic TWL components accurately represent the observational TWL components, there are several possible improvements to the approach. We have modeled η_{NTRs} directly, however, they are comprised of both high (e.g., storm surge) and low-frequency (e.g., monthly mean sea level anomalies) processes that modify water levels. Splitting the η_{NTR} into low and high-frequency signals [*Méndez et al.*, 2007; *Merrifield et al.*, 2013] would perhaps provide better extreme value distribution fits [*Méndez et al.*, 2007]. Modeling the conditional dependency between a high-frequency η_{NTR} component and SWH also may result in a stronger relationship between the two since their drivers are more closely related. Initial results suggest splitting up these components allows for more climate variability to be explained. Currently, we do not take into account any autocorrelation when modeling climate variability through

Table 3. Total Water Level (TWL) Return Level Estimates and Corresponding Confidence Intervals[a]

Return Period (year)	Return Levels (m)	
	Observational (CI)	TWL-FSM (CI)
10	6.47 (0.25)	6.67 (0.16)
25	6.73 (0.36)	6.94 (0.16)
50	6.91 (0.45)	7.17 (0.26)
100	7.08 (0.56)	7.37 (0.26)
500	7.43 (0.83)	7.70 (0.37)

[a]Return level estimates are for a representative transect in the Rockaway, Oregon littoral cell with a beach slope of approximately 0.04. Waves have been shoaled to just before breaking and then reverse-shoaled back to deep water for the empirical runup parameterization.
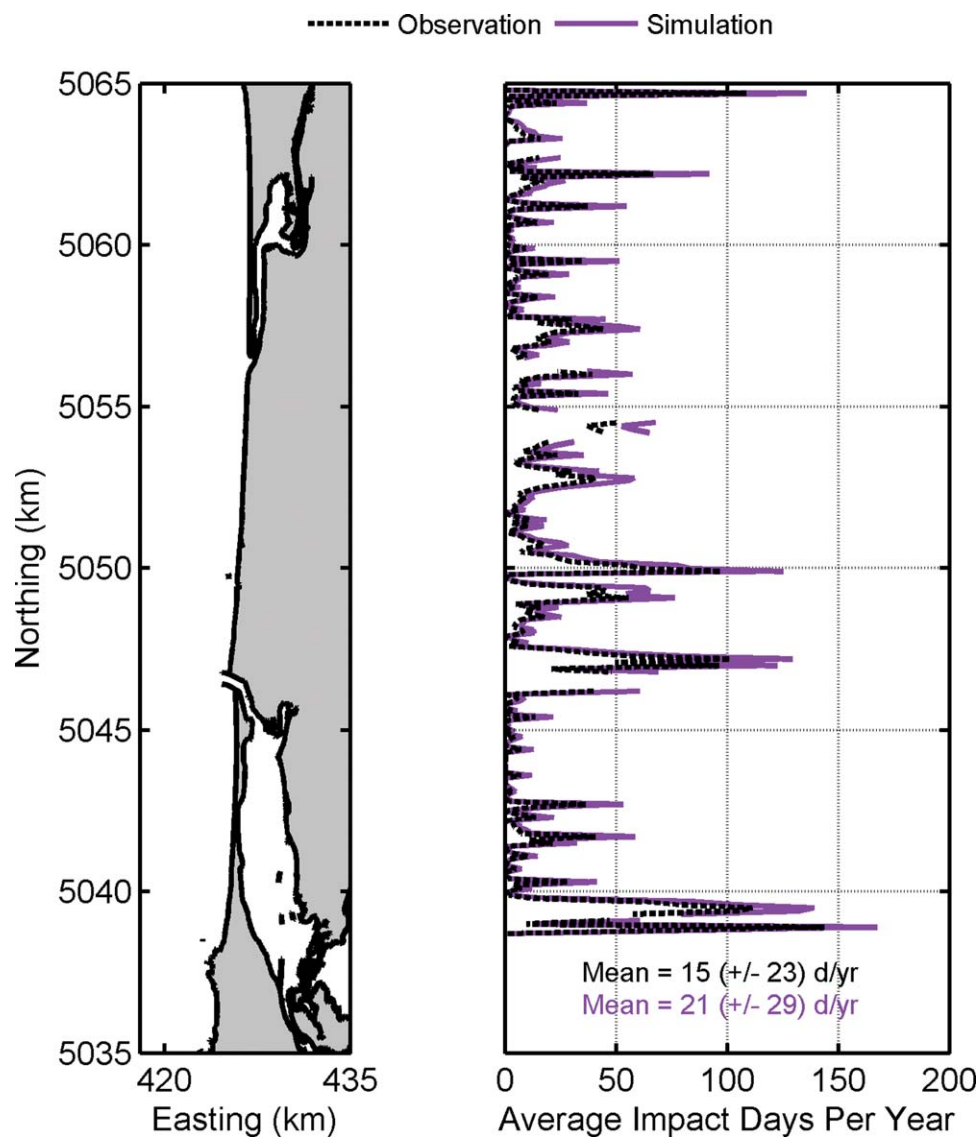
Figure 15. Longshore variability of impact days per year (IDPY) in the Rockaway littoral cell. Alongshore averaged IDPY for the daily "observational" record are 15 ($\pm$23) while alongshore averaged IDPY increases to 21($\pm$29) using the simulated data.

climate indices. Despite representing the frequency of El Niño and La Niña years correctly, we miss out on the occurrence of back-to-back events, important for understanding the extent of coastal erosion. Future work will focus on modeling the climate indices as Markov sequences to include this important autocorrelation.

The TWL-FSM does an appropriate job capturing the amount of data in extreme space (1.4% and 1.38%, "observed"; 1.27% and 1.36%, simulated; η_{NTR} and SWH, respectively), however, estimates of concurrent extremes are biased low (0.61%, "observed"; 0.31%, simulated, upper right quadrant in Figure 11 top left). Since the dependency parameter, α, partially governs the co-occurrence of extremes, we examine the influence of this parameter on the amount of simulations that fall into this quadrant. By lowering the dependency parameter to 0.7 and 0.6 (i.e., more dependent than our computed value of 0.83), we find better agreement in the concurrent extreme quadrant (0.5% and 0.65%, respectively). The dependency parameter is also inversely related to the elevation of TWL return level events—the smaller α, the higher the return level estimate (100 year TWL return level: $\sim$7.98 m for $\alpha = 0.83$; $\sim$8.01 m for $\alpha = 0.7$; $\sim$8.15 m for $\alpha = 0.6$; computed using deep-water conditions). While the logistics model used here (equation (9)) captures some of the
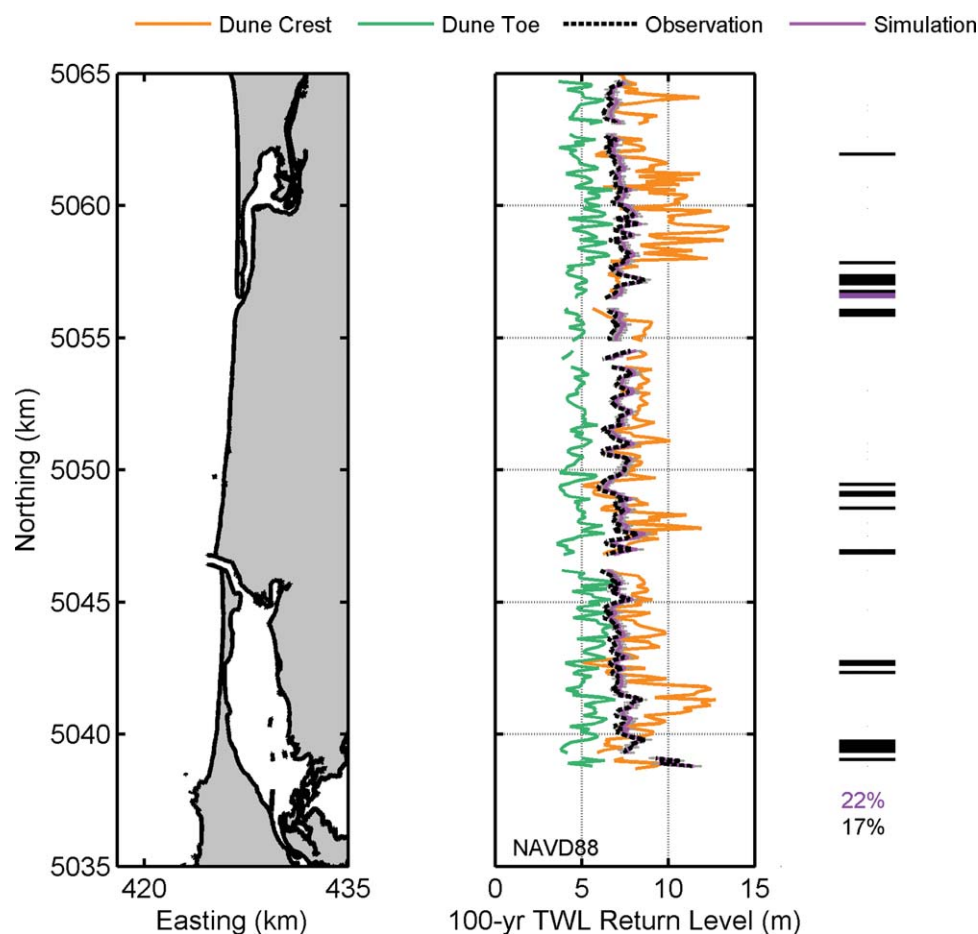
Figure 16. Longshore variability of the 100 year TWL return level event in the Rockaway littoral cell. The average 100 year TWL return level event across the 50 simulations results in 30% more of the coastline being overtopped than the daily "observational" record indicates. The bars to the right indicate the locations that the extreme TWL estimates overtop the dune crest.

dependency between η_{NTR} and SWH, it may not appropriately capture the seasonal to interannual dependence between events. Therefore, we may be able to create more realistic representations of the dependency between SWH and η_{NTR}, and a better agreement in the percentage of concurrent extreme SWH and η_{NTR}, using both a time-varying α and threshold estimates for the POT [*Coles et al.*, 1994]. Better extreme value distribution fits and conditional dependency fits would provide a more accurate representation of extreme events, therefore improving our overall TWL return level estimates.

In order to account for the uncertainty in the GPD-Poisson parameter estimates of the extremes (and the log-normal or logistic distribution parameter estimates of the nonextreme data), we sample from the standard error estimates around the best model fit, allowing each simulation to sample from slightly different SWH and η_{NTR} distributions. This inclusion of uncertainty has a minimal effect on the TWL return level estimates, increasing estimates by <10 cm and widening the confidence bounds only slightly. However, the confidence bounds are still narrower than those produced by the "observational" extreme TWL estimates. There is additional uncertainty, related to other parameters, which could be included in the TWL-FSM. For example, the Stockdon parameterization of $R_{2\%}$ has an RMSE of ~20 cm, which can be added to the bounds of computed runup during simulations. We do not include this uncertainty for this application since it would be present in both the "observational" and simulated records and therefore would not contribute to a difference in extreme TWLs.

Some stretches along the Rockaway littoral cell are backed by hard coastal protection structures. While in this application we have used the *Stockdon et al.* [2006] parameterization for wave runup throughout the littoral cell, it may not be the most appropriate formulation for these protected beaches as it was derived solely from data collected on sandy beaches. Other approaches for computing wave runup on rubble
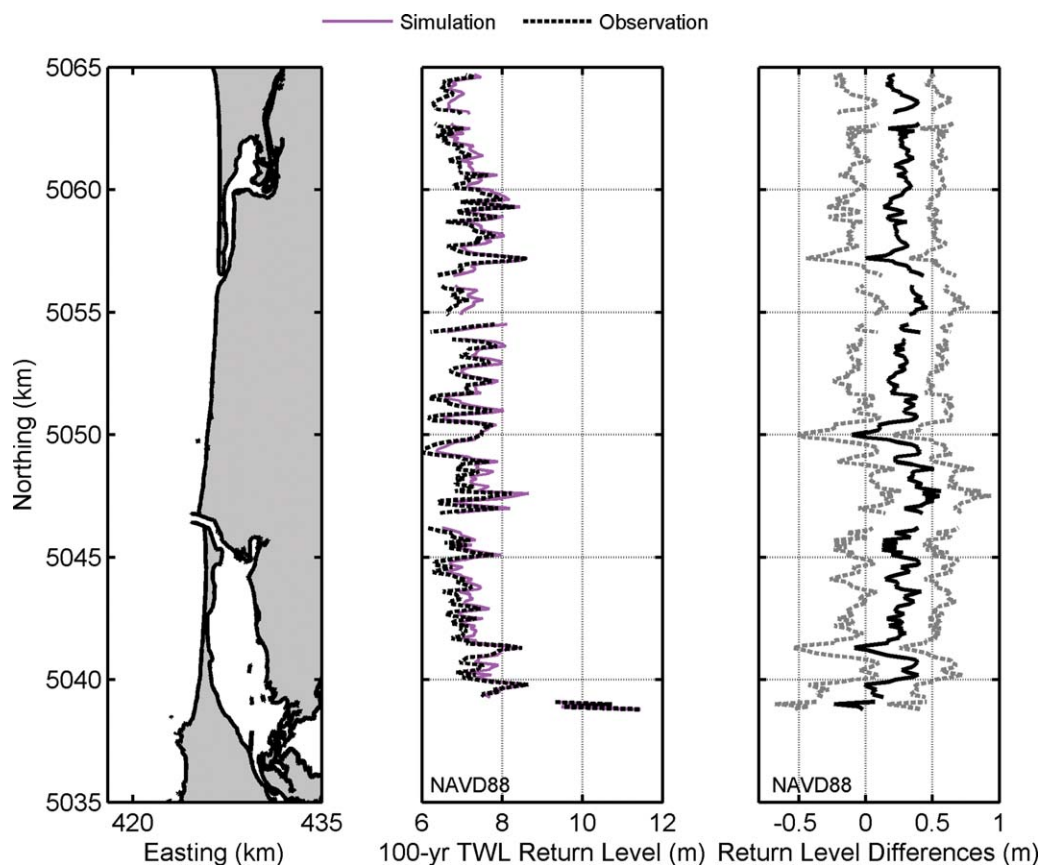
Figure 17. Longshore variability of the difference between the TWL-FSM and "observational" 100 year TWL return level across the Rockaway littoral cell (plot 3). Hashed gray lines display the difference between the maximum (and minimum) simulated 100 year TWL return level and "observational" 100 year TWL return level.

mound structures [e.g., *van der Meer and Stam*, 1992; *Hughes*, 2004] or vertical seawalls [*van der Meer*, 2002] exist and could be implemented into the methodology. Perhaps more importantly, the geomorphology of the coast is constantly evolving, while the parameters used here to evaluate coastal hazards (beach slope, dune crest elevation, and dune toe elevation), were extracted from a single lidar flight in 2002. Therefore, to create a more accurate representation of flood and erosion hazard risk, the variability of beach and dune morphology could be accounted for either through probabilistic techniques or numerical modeling. The approaches used here to simplify the problem are similar to techniques used in *Callaghan et al.* [2008] and *Gouldby et al.* [2014] for modeling erosion.

The TWL-FSM produces synthetic records that are an accurate representation of our "observational" record. The approach has been designed such that it easily accommodates any possible continued changes to the various components of TWLs in a future climate. The historical records in our region of model application (U.S. PNW) not only show relative sea level change [*Komar et al.*, 2011] but also increasing trends in SWHs [*Allan and Komar*, 2000; *Ruggiero et al.*, 2010; *Méndez et al.*, 2010]. Projections of future sea level changes, possible changes to the wave climate, and changes in ENSO variability, are at present quite uncertain [e.g., *National Research Council*, 2012; *Hemer et al.*, 2013; *Santoso et al.*, 2013; *Wang et al.*, 2014], and at this point little is known about how these changes will impact overall TWLs [*Ruggiero*, 2013]. Our ongoing work will therefore focus on investigating the impacts of future climate scenarios on TWLs, using a range of approaches including both statistical [e.g., *Izaguirre et al.*, 2012; *Wang et al.*, 2014] and dynamical [e.g., *Hemer et al.*, 2013] downscaling approaches.

5. Conclusions

This paper presents the TWL-FSM, a full simulation, probabilistic TWL model that captures the seasonal and interannual climatic variability in extreme events. This full simulation approach includes the following steps:

the simulation of climate indices representing alternate realizations of the climate record; the simulation of extreme SWH and η_{NTR} from a nonstationary GPD-Poisson model that includes the conditional dependency between the two, or, for nonextreme conditions, from distributions based on lognormal or logistic distribution fits, respectively; the simulation of T_p based on the conditional dependency between T_p and SWH; and the simulation of other key components for producing TWLs, for example, the tide and MWD.

Our simulations capture a wider variety of extreme events that while not necessarily occurring in the "observational" record are certainly physically capable of occurring based on present-day TWL component distributions. In an application of the full simulation model to a representative littoral cell in the U.S. PNW, the TWL-FSM results in 100 year TWL return levels on average 30 cm (but as large as 90 cm) higher than TWL return levels estimated from the independent "observational" record. The amount of time that dunes are subjected to erosive processes increases approximately 40%, while the amount of coastline affected by overtopping during the 100 year TWL return level event increases by approximately 30%. TWLs are simulated using present-day conditions; therefore, any increase in return levels is due to both the larger variation of SWH, T_p, and MWD combinations and resulting transformation to the nearshore, ENSO variability, and to the random chance of co-occurring high wave and sea level events. Robust estimates of design storm events are necessary for design of coastal defenses and flood hazard risk assessment, and the full simulation approach improves upon these estimates by narrowing confidence bounds around extreme events. While our ongoing research is focusing on incorporating future climate scenarios into this model, the method advances the current understanding of extreme TWL return levels in the PNW by allowing for more robust estimates of extreme TWLs, and therefore, improving knowledge of coastal risks.

References

Akaike, H. (1974), A new look at the statistical model identification, *IEEE Trans. Autom. Control*, *19*(6), 716–723.

Allan, J., and P. D. Komar (2000), Are ocean wave heights increasing in the eastern North Pacific?, *Eos Trans. AGU*, *81*(47), 561–567.

Allan, J. C., and P. D. Komar (2002), Extreme storms on the Pacific Northwest coast during the 1997-98 El Nino and 1998-99 La Nina, *J. Coastal Res.*, *18*, 175–193.

Allan, J. C., P. D. Komar, and P. Ruggiero (2011), Storm surge magnitudes and frequency on the central Oregon coast, in edited by L. Wallendorf, C. Jones, L. Ewing, and B. Battalio, *Proceedings of the 2011 Solutions to Coastal Disasters Conference*, pp. 53–64, ASCE, Anchorage, Alaska, doi:10.1061/41185(417)6.

Allan, J. C., P. Ruggiero, and J. T. Roberts (2012), *Coastal Flood Insurance Study*, Oregon Dep. of Geol. and Miner. Ind., Coos County, Oreg.

Booij, N., R. Ris, and L. H. Holthuijsen (1999), A third-generation wave model for coastal regions: 1. Model description and validation, *J. Geophys. Res.*, *104*(C4), 7649–7666.

Bromirski, P. D., R. E. Flick, and D. R. Cayan (2003), Storminess variability along the California coast: 1858–2000, *J. Clim.*, *16*(6), 982–993.

Burgette, R. J., R. J. Weldon, and D. A. Schmidt (2009), Interseismic uplift rates for western Oregon and along-strike variation in locking on the Cascadia subduction zone, *J. Geophys. Res.*, *114*, B01408, doi:10.1029/2008JB005679.

Cai, W., et al. (2014), Increasing frequency of extreme El Niño events due to greenhouse warming, *Nat. Clim. Change*, *4*, 111–116.

Callaghan, D., P. Nielsen, A. Short, and R. Ranasinghe (2008), Statistical simulation of wave climate and extreme beach erosion, *Coastal Eng.*, *55*(5), 375–390.

Cazenave, A., H.-B. Dieng, B. Meyssignac, K. von Schuckmann, B. Decharme, and E. Berthier (2014), The rate of sea-level rise, *Nat. Clim. Change*, *4*, 358–361, doi:10.1038/nclimate2159.

Church, J. A., and N. J. White (2006), A 20th century acceleration in global sea-level rise, *Geophys. Res. Lett.*, *33*, L01602, doi:10.1029/2005GL024826.

Church, J. A., and N. J. White (2011), Sea-level rise from the late 19th to the early 21st century, *Surv. Geophys.*, *32*(4-5), 585–602.

Coles, S. G. (2001), *An Introduction to Statistical Modeling of Extreme Values*, vol. 208, Springer, London, U. K.

Coles, S. G., J. A. Tawn and R. L. Smith (1994), A seasonal Markov model for extremely low temperatures, *Environmetrics*, *5*, 221–239.

Corbella, S., and D. D. Stretch (2013), Simulating a multivariate sea storm using Archimedean copulas, *Coastal Eng.*, *76*, 68–78.

Crowell, M., S. Edelman, K. Coulton, and S. McAfee (2007), How many people live in coastal areas?, *J. Coastal Res.*, *23*(5), iii–vi.

Crowell, M., K. Coulton, C. Johnson, J. Westcott, D. Bellomo, S. Edelman, and E. Hirsch (2010), An estimate of the US population living in 100-year coastal flood hazard areas, *J. Coastal Res.*, *26*, 201–211.

Davison, A. C., and D. V. Hinkley (1997), *Bootstrap Methods and Their Application*, Cambridge Univ. Press, Cambridge, U. K.

Davison, A. C., and R. L. Smith (1990), Models for exceedances over high thresholds, *J. R. Stat. Soc., Ser. B*, *52*, 393–442.

Efron, B., and R. J. Tibshirani (1993), *An Introduction to the Bootstrap*, Chapman and Hall, N. Y.

Emanuel, K. A. (2013), Downscaling CMIP5 climate models shows increased tropical cyclone activity over the 21st century, *Proc. Natl. Acad. Sci. U. S. A.*, *110*(30), 12219–12224.

García-Medina, G., H. Özkan-Haller, P. Ruggiero, and J. Oskamp (2013), An inner-shelf wave forecasting system for the US Pacific northwest, *Weather Forecasting*, *28*(3), 681–703.

Garrity, N. J., R. Battalio, P. J. Hawkes, and D. Roupe (2006), Evaluation of event and response approaches to estimate the 100-year coastal flood for Pacific coast sheltered waters, in *Proceedings of the 30th International Conference on Coastal Engineering*, pp. 1651–1663, World Scientific, San Diego, Calif.

Geman, S., and D. Geman (1984), Stochastic relaxation, Gibbs distributions, and the Bayesian restoration of images, *IEEE Trans. Pattern Anal. Mach. Intel.*, *6*(6), 721–741.

Goring, D., S. Stephens, R. Bell, and C. Pearson (2010), Estimation of extreme sea levels in a tide-dominated environment using short data records, *J. Waterway Port Coastal Ocean Eng.*, *137*(3), 150–159.

Gouldby, B., F. Méndez, Y. Guanche, A. Rueda, and R. Mínguez (2014), A methodology for deriving extreme nearshore sea conditions for structural design and flood risk analysis, *Coastal Eng.*, *88*, 15–26.

Graham, N. E., and H. F. Diaz (2001), Evidence for intensification of North Pacific winter cyclones since 1948, *Bull. Am. Meteorol. Soc.*, *82*(9), 1869–1893.

Gumbel, E. J. (1958), *Statistics of Extremes*, Columbia University Press, N. Y.

Haigh, I. D., E. Wijeratne, L. R. MacPherson, C. B. Pattiaratchi, M. S. Mason, P. P. Crompton, and S. George (2013), Estimating present day extreme water level exceedance probabilities around the coastline of Australia: Tides, extra-tropical storm surges and mean sea level, *Clim. Dyn.*, *42*(1-2), 121–138.

Hasselmann, K., W. Sell, D. B. Ross, and P. Müller (1976), A parametric wave prediction model, *J. Phys. Oceanogr.*, *6*(2), 200–228.

Hawkes, P. J., B. P. Gouldby, J. A. Tawn, and M. W. Owen (2002), The joint probability of waves and water levels in coastal engineering design, *J. Hydraul. Res.*, *40*(3), 241–251.

Hemer, M. A., Y. Fan, N. Mori, A. Semedo, and X. L. Wang (2013), Projected changes in wave climate from a multi-model ensemble, *Nat. Clim. Change*, *3*(5), 471–476.

Holman, R. A., and A. Sallenger (1986), Setup and swash on a natural beach, *J. Geophys. Res.*, *90*(C1), 945–953.

Hughes, S. A. (2004), Estimation of wave run-up on smooth, impermeable slopes using the wave momentum flux parameter, *Coastal Eng.*, *51*(11), 1085–1104.

Izaguirre, C., M. Menéndez, P. Camus, F. J. Méndez, R.Mínguez, and I. J. Losada (2012), Exploring the interannual variability of extreme wave climate in the Northeast Atlantic Ocean, *Ocean Modell.*, *59*, 31–40.

Katz, R. W., M. B. Parlange, and P. Naveau (2002), Statistics of extremes in hydrology, *Adv. Water Res.*, *25*(8), 1287–1304.

Knutson, T. R., J. L. McBride, J. Chan, K. Emanuel, G. Holland, C. Landsea, I. Held, J. P. Kossin, A. K. Srivastava, and M. Sugi (2010), Tropical cyclones and climate change, *Nat. Geosci.*, *3*(3), 157–163.

Komar, P. D. (1998), *The Pacific Northwest Coast: Living With the Shores of Oregon and Washington*, 195 pp., Duke Univ. Press, Durham, NC.

Komar, P. D., and D. B. Enfield (1987), Short-term sea-level changes and coastal erosion, in *Sea-Level Fluctuation and Coastal Evolution, Spec. Publ.*, vol. 41, pp 17–27, Soc. of Econ. Paleontol. and Mineral, Tulsa, Okla.

Komar, P. D., J. C. Allan, and P. Ruggiero (2011), Sea level variations along the US Pacific Northwest coast: Tectonic and climate controls, *J. Coastal Res.*, *27*(5), 808–823.

Leadbetter, M., G. Lindgren, and H. Rootzen (1983), *Extremes and Related Properties of Random Sequences and Processes*, Springer, Berlin.

Li, F., P. van Gelder, R. Ranasinghe, D. Callaghan, and R. Jongejan (2014), Probabilistic modelling of extreme storms along the Dutch coast, *Coastal Eng.*, *86*, 1–13.

Longuet-Higgins, M. S., and R. Stewart (1963), A note on wave set-up, *J. Mar. Res.*, *21*, 4–10.

Longuet-Higgins, M. S., and R. Stewart (1964), Radiation stresses in water waves; a physical discussion, with applications, *Deep Sea Res. Oceanogr. Abstr.*, *11*, 529–562.

Madsen, H., C. P. Pearson, and D. Rosbjerg (1997a), Comparison of annual maximum series and partial duration series methods for modeling extreme hydrologic events: 2. Regional modeling, *Water Resour. Res.*, *33*(4), 759–769.

Madsen, H., C. P. Pearson, and D. Rosbjerg (1997b), Comparison of annual maximum series and partial duration series methods for modeling extreme hydrologic events: 1. At-site modeling, *Water Resour. Res.*, *33*(4), 747–757.

McCullagh, P., and J. Nelder (1989), *Generalized Linear Models*, Chapman and Hall, London, U. K.

Méndez, F. J., M. Menéndez, A. Luceño, and I. J. Losada (2006), Estimation of the long-term variability of extreme significant wave height using a time-dependent Peak Over Threshold (POT) model, *J. Geophys. Res.*, *111*, C07024, doi:10.1029/2005JC003344.

Méndez, F. J., M. Menéndez, A. Luceño, and I. J. Losada (2007), Analyzing monthly extreme sea levels with a time-dependent GEV model, *J. Atmos. Oceanic Technol.*, *24*(5), 894–911.

Méndez, F. J., M. Menéndez, A. Luceño, R. Medina, and N. E. Graham (2008), Seasonality and duration in extreme value distributions of significant wave height, *Ocean Eng.*, *35*(1), 131–138.

Méndez, F. J., C. Izaguirre, M. Menéndez, B. G. Reguero, and I. J. Losada (2010), Is the extreme wave climate in the NE Pacific increasing?, *Proceedings of Oceans 2010*, pp. 1–7, MTS/IEEE, Seattle, Wash.

Menéndez, M., and P. L. Woodworth (2010), Changes in extreme high water levels based on a quasi-global tide-gauge data set, *J. Geophys. Res.*, *115*, C10011, doi:10.1029/2009JC005997.

Menéndez, M., F. J. Méndez, C. Izaguirre, A. Luceño, and I. J. Losada (2009), The influence of seasonality on estimating return values of significant wave height, *Coastal Eng.*, *56*(3), 211–219.

Merrifield, M. A., A. S. Genz, C. P. Kontoes, and J. J. Marra (2013), Annual maximum water levels from tide gauges: Contributing factors and geographic patterns, *J. Geophys. Res. Oceans*, *118*, 2535–2546, doi:10.1002/jgrc.20173.

Milly, P., J. Betancourt, M. Falkenmark, R. Hirsch, W. Zbigniew, D. Lettenmaier, and R. Stouffer (2008), Stationarity is dead: Whither water management?, *Science*, *319*(5863), 573–574.

Mull, J., and P. Ruggiero (2014), Estimating storm-induced dune erosion and overtopping along U.S. West Coast beaches, *J. Coastal Res.*, doi:10.2112/JCOASTRES-D-13-00178.1, in press.

National Research Council (2012), *Sea-Level Rise for the Coasts of California, Oregon, and Washington: Past, Present, and Future*, Comm. on Sea Level Rise in Calif., Oreg., and Wash.; Board on Earth Sci. and Resour.; Ocean Stud. Board; Div. on Earth and Life Stud., The National Academies Press, Washington, D. C.

NOAA Coastal Services Center (2002), 2002 NASA/USGS Airborne LiDAR Assessment of Coastal Erosion (ALACE) Project for California, Oregon, and Washington Coastlines, NOAA's Ocean Serv., Coastal Serv. Cent. Charleston, S. C. [Available at http://www.csc.noaa.gov/digitalcoast.]

Pickands, J., III (1975), Statistical inference using extreme order statistics, *Ann. Stat.*, *3*, 119–131.

Plant, N. G., K. T. Holland, and J. A. Puleo (2002), Analysis of the scale of errors in nearshore bathymetric data, *Mar. Geol.*, *191*(1), 71–86.

Pugh, D. T. (1987), *Tides, Surges and Mean Sea-Level*, John Wiley & Sons, Chichester, U. K.

Raubenheimer, B., R. Guza, and S. Elgar (2001), Field observations of wave-driven setdown and setup, *J. Geophys. Res.*, *106*(C3), 4629–4638.

Ruggiero, P. (2013), Is the intensifying wave climate of the US Pacific northwest increasing flooding and erosion risk faster than sea-level rise?, *J. Waterway Port Coastal Ocean Eng.*, *139*(2), 88–97.

Ruggiero, P., P. Komar, W. McDougal, and R. Beach (1996), Extreme water levels, wave runup and coastal erosion, in *Proceedings 25th International Coastal Engineering Conference* (ASCE), *1*(25), pp. 2793–2805.

Ruggiero, P., P. D. Komar, W. G. McDougal, J. J. Marra, and R. A. Beach (2001), Wave runup, extreme water levels and the erosion of properties backing beaches, *J. Coastal Res.*, *17*, 407–419.

Ruggiero, P., P. D. Komar, and J. C. Allan (2010), Increasing wave heights and extreme value projections: The wave climate of the US Pacific Northwest, *Coastal Eng.*, *57*(5), 539–552.

Ruggiero, P., M. G. Kratzmann, E. S. Himmelstoss, D. Reid, J. Allan, and G. Kaminsky (2013), National assessment of shoreline change—Historical shoreline change along the Pacific Northwest coast, *U.S. Geol. Surv. Open File Rep., 2012-1007*, 62 pp., doi:10.3133/ofr20121007.

Sallenger, A. H., Jr. (2000), Storm impact scale for barrier islands, *J. Coastal Res.*, *16*, 890–895.

Sallenger, A. H., Jr., K. S. Doran and P. A. Howd (2012), Hotspot of accelerated sea-level rise on the Atlantic coast of North America, *Nat. Clim. Change*, *2*(12), 884–888.

Santoso, A., S. McGregor, F.-F. Jin, W. Cai, M. H. England, S.-I. An, M. J. McPhaden, and E. Guilyardi (2013), Late-twentieth-century emergence of the El Nino propagation asymmetry and future projections, *Nature*, *504*(7478), 126–130.

Smith, R. (2001), Extreme value statistics in meteorology and the environment, *Environ. Stat.*, *8*, 300–357.

Smith, R. L. (1986), Extreme value theory based on the r largest annual events, *J. Hydrol.*, *86*(1), 27–43.

Smith, R. L. (1989), Extreme value analysis of environmental time series: An application to trend detection in ground-level ozone, *Stat. Sci.*, *4*(4), 367–377.

Stenseth, N. C., G. Ottersen, J. W. Hurrell, A. Mysterud, M. Lima, K.-S. Chan, N. G. Yoccoz, and B. Ådlandsvik (2003), Studying climate effects on ecology through the use of climate indices: The North Atlantic Oscillation, El Nino Southern Oscillation and beyond, *Proc. R. Soc. London, Ser. B*, *270*(1529), 2087–2096.

Stockdon, H. F., R. A. Holman, P. A. Howd, and A. H. Sallenger Jr. (2006), Empirical parameterization of setup, swash, and runup, *Coastal Eng.*, *53*(7), 573–588.

Stockdon, H. F., K. S. Doran, and A. H. Sallenger Jr.(2009), Extraction of lidar-based dune-crest elevations for use in examining the vulnerability of beaches to inundation during hurricanes, *J. Coastal Res.*, *SI*(53), 59–65.

Tawn, J. A. (1988), Bivariate extreme value theory: Models and estimation, *Biometrika*, *75*(3), 397–415.

van der Meer, J. (2002), Technical report: wave run-up and wave overtopping at dikes, technical report, 43 pp., Tech. Advis. Comm. on Flood Def, Delft, Netherlands.

van der Meer, J. W., and C.-J. M. Stam (1992), Wave runup on smooth and rock slopes of coastal structures, *J. Waterway Port Coastal Ocean Eng.*, *118*(5), 534–550.

Wang, X. L., Y. Feng, and V. Swail (2014), Changes in global ocean wave heights as projected using multimodel CMIP5 simulations, *Geophys. Res. Lett.*, *41*, 1026–1034, doi:10.1002/2013GL058650.

Woodruff, J. D., J. L. Irish, and S. J. Camargo (2013), Coastal flooding by tropical cyclones and sea-level rise, *Nature*, *504*(7478), 44–52.

Zhang, H., and J. Sheng (2013), Estimation of extreme sea levels over the eastern continental shelf of North America, *J. Geophys. Res. Oceans*, *118*, 6253–6273, doi:10.1002/2013JC009160.